

The “Rebound Controversy”: An Overview and Theoretical Modeling of the Rebound Step in C–H Hydroxylation by Cytochrome P450

Sason Shaik,^{*,[a]} Shimrit Cohen,^[a] Samuël P. de Visser,^[a] Pankaz K. Sharma,^[a]
Devesh Kumar,^[a] Sebastian Kozuch,^[a] François Ogliaro,^[a] and David Danovich^[a]

Dedicated to H. F. (Fritz) Schaefer, a friend and a great scientist, on the occasion of his 60th birthday

Keywords: Alkanes / Cytochrome P450 / Density functional calculations / Enzyme catalysis / Free radicals / C–H hydroxylation

C–H hydroxylation by the enzyme cytochrome P450 is one of Nature's important and most ubiquitous processes. There is strong evidence that the mechanism proceeds by initial hydrogen abstraction, from the alkane, by the high-valent iron–oxo species of the enzyme, followed by a rebound of the alkyl radical to form the ferric–alcohol product complex (the Groves “rebound” mechanism). Nevertheless, the “rebound” mechanism is still controversial due to the ultrashort radical lifetimes deduced from radical-clock experiments. This review describes the main elements of the controversy and its updated resolution by theory, with an emphasis on the controversial rebound step. The theoretically derived model for alkane hydroxylation is found to involve two-state reactivity (TSR). In TSR, radicals are produced on two different spin-state surfaces, and thereafter they react differently; on the low-spin surface, the rebound proceeds with no product rearrangement and the lifetime of the radicals is ultrashort (or

zero), while on the high-spin surface the barrier for rebound is substantial and the lifetime of the radical is sufficiently long that rearrangement may compete with product formation by rebound. A new valence-bond model is developed to model the rebound barrier on the high-spin surface and conceptualize its dependence on the nature of the alkyl radical. The possible intermediacy of carbocationic intermediates alongside radicals is discussed. It is shown that the TSR scenario provides a satisfactory rationale for the controversial findings in the field, and makes verifiable predictions. One of the predictions of TSR is that the ratio of unrearranged to rearranged products, $[U/R]$, will be subject to an intrinsic isotope effect that is substrate-dependent. This prediction and its possible verification by experiment are discussed.

(© Wiley-VCH Verlag GmbH & Co. KGaA, 69451 Weinheim, Germany, 2004)

Introduction

Cytochrome P450, one of Nature's most potent monooxygenating enzymes in aerobic organisms,^[1] has an oxidizing domain that consists of an iron–protoporphyrin complex, Figure 1, held by the protein through salt bridges to the propionate substituents and via a cysteinate (CysS) axial ligand — the “proximal ligand” — which is part of the encapsulating protein. Entrance of a substrate, RH, triggers a succession of events, which include dioxygen uptake, re-

duction and protonation, all of which activate the oxidase domain and convert the iron–porphyrin complex into the active species of the enzyme, the high-valent iron–oxo species called Compound I (Cpd I; Figure 1). Some of the most important functions of the enzyme involve the hydroxylation of alkanes to alcohols. As stated in the title, this paper focuses on the recent controversy that surrounds the rebound mechanism of alkane hydroxylation, and in particular on the key step of this mechanism, the rebound step itself.

In 1976 Groves and McCluskey^[2] suggested that alkane (Alk–H) hydroxylation by P450 proceeds by a rebound mechanism (Scheme 1). The first step in this mechanism involves hydrogen abstraction from the alkane by Cpd I. Subsequently, the alkyl radical is partitioned between two competing processes. It can either instantly rebound to form an alcohol complex, where the alcohol is unrearranged (U),

^[a] Department of Organic Chemistry and the Lise Meitner–Minerva Center for Computational Quantum Chemistry, The Hebrew University of Jerusalem, Givat Ram Campus, 91904 Jerusalem, Israel
Fax: (internat.) + 972-2-658-4680
E-mail: sason@yfaat.ch.huji.ac.il

Supporting information for this article is available on the WWW under <http://www.eurjic.org> or from the author.

MICROREVIEWS: This feature introduces the readers to the author's research through a concise overview of the selected topic. Reference to important work from others in the field is included.

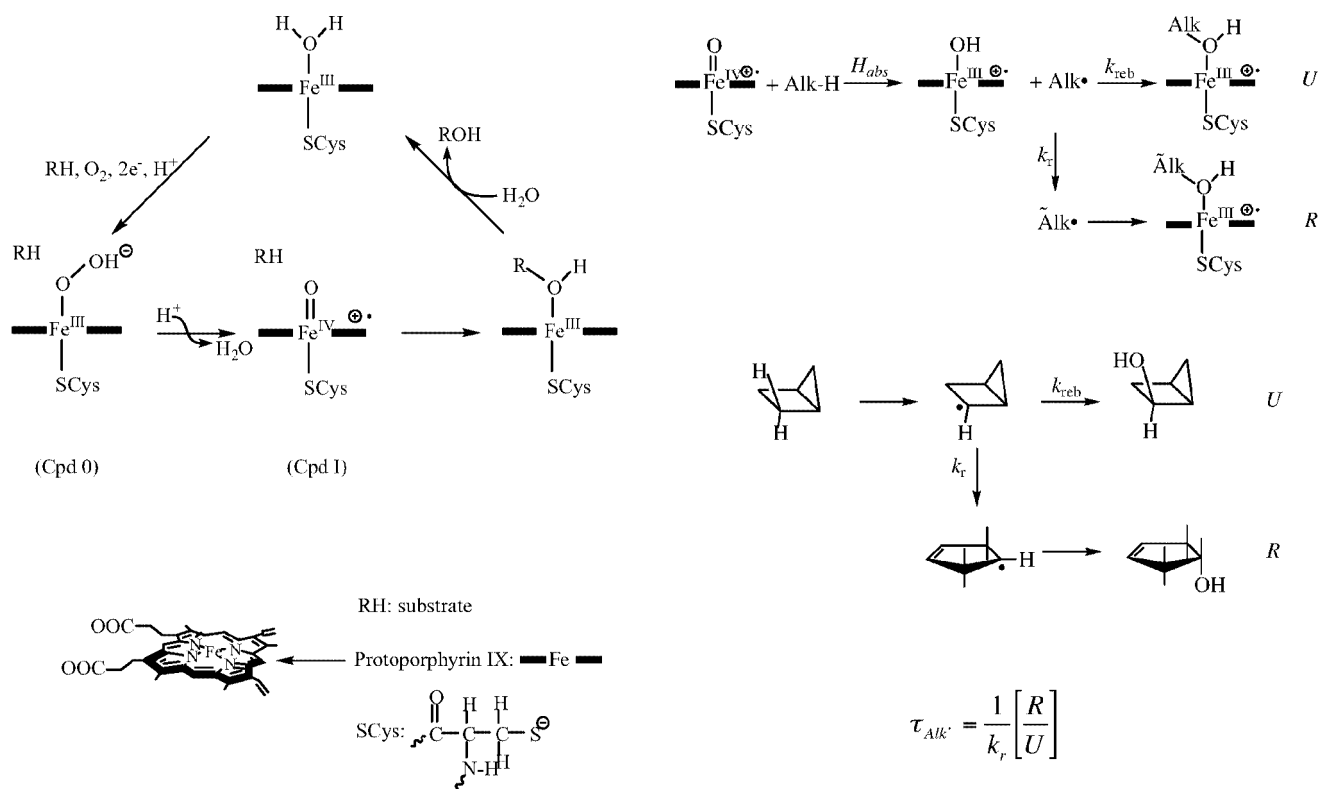


Figure 1. A truncated catalytic cycle of the enzyme cytochrome P450, showing the resting state, the active species Cpd I, its precursor, Cpd 0, and the initial product of alkane hydroxylation, the alcohol complex

keeping the original stereochemical information possessed by the alkane, or it can first undergo skeletal rearrangement and then rebound to give a rearranged (*R*) alcohol product. The rebound mechanism accounts for the partial loss of

Scheme 1. The rebound mechanism, and the results of hydroxylation of bicyclo[2.1.0]pentane (ref.^[12])

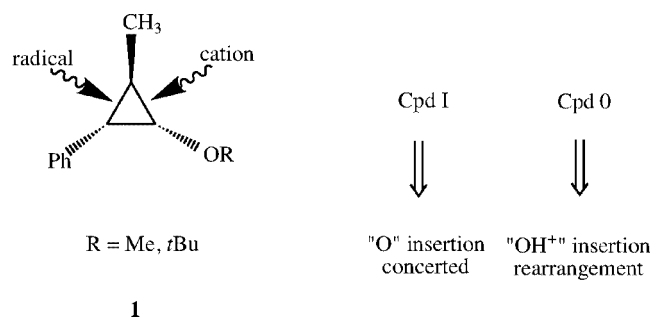
stereochemistry and geometrical rearrangement data,^[3] as well as for the large kinetic isotope effect (KIE) observed^[4–10] when the hydrogen atom of the scissible C–H bond is replaced by a deuterium atom. However, the large degree of stereoselectivity (> 90%) and the sometimes completely stereospecific^[8,11] hydroxylation suggested that the radicals are rather short-lived.

The Research Group in The Hebrew University: This Microreview summarizes the story of six years of intensive scientific discourse in the attempt to resolve the “rebound controversy” in the C–H hydroxylation chemistry by cytochrome P450. Our group entered the research on heme enzymes through the crack provided by the tiny FeO⁺ diatomic that mimics the ability of cytochrome P450 to hydroxylate C–H bonds. This small diatomic posed some very enticing puzzles: the reaction with hydrocarbons was highly exothermic, apparently spin-allowed, and certainly orbitally allowed. Despite these rosy prospects, the efficiency of the reaction was extremely poor! The solution of this puzzle, together with Helmut Schwarz and Detlef Schröder, led to the development of the idea of two-state reactivity, TSR (ref.^[26]), which is gaining increasing popularity in the community. Already then there was something in the air of P450 literature that spelled TSR. The “rebound controversy” was reminiscent of some TSR features, the intellectual dilemma it posed was challenging, and the chance for a scientific discourse was appealing. Our foray into the field was rather modest (ref.^[33]). The three postdocs who started us off, Michael Filatov (now in Goteborg), Nathan Harris (now with Chemical Abstracts), and François Ogliaro (now in Kings College, London) were soon joined by other co-workers who are still in the group in Jerusalem, Sam de Visser (a Dutch postdoc from Amsterdam), Pankaz K. Sharma (an Indian postdoc from Hyderabad), Devesh Kumar (an Indian postdoc from Gorakhpur), Shimrit Cohen (a Ph.D. student from Jerusalem), Sebastian Kozuch (a Ph.D. student, a new immigrant from Argentina, now an M.Sc. student in Jerusalem), and David Danovich (a senior research associate, in the group since 1992). At present, the group has grown by three more postdocs and one graduate student.

The field of P450 is a vast ocean of many waters. Besides its being an intellectual arena full with enticing puzzles waiting to be solved, it is also an interdisciplinary field that is nestled in the crossroads between chemistry, biology, physics and medicine. Being active in such a field requires maintenance of many dialogues, and our group has been fortunate to enjoy and benefit from useful discussions with chemists and biologists of variegated expertise; Bernard Meunier, John Dawson, Joe Dinnocenzo, Sunichi Fukuzumi, Mike Green, Zeev Gross, Jay Groves, Fred Guengrich, Danni Harris, Jeff Jones, Isao Morishima, Marty Newcomb, Paul Ortiz de Montellano, Tom Poulos, Steve Sligar, Yoshi Watanabe, Wolf-D. Woggon, Kazunari Yoshizawa, Hendrik Zipse, and others in the heme enzyme community. As a group of theoretical chemistry, we have initially used only quantum mechanics (QM). Some controversies in the description of the active species of the enzyme by different QM modeling methods led us to the development of the concept of chameleon oxidants (ref.^[27]), and very quickly it was evident that we must master also hybrid quantum mechanics/molecular mechanics (QM/MM) calculation since they enable to account for the effect of the protein environment. This is done in a fruitful and ongoing collaboration (ref.^[46]) with Walter Thiel and his group members, Jan Schöneboom and Natalie Reuter (from the Max Planck Institute in Mülheim). We are even beginning to enjoy some docking calculations, and appreciate the importance of the protein motions that Judith Klinman talks about. Indeed, the field of heme enzymes has offered much more than initially expected in the fall of 1997, when I (S. S.) drew the active species of P450 for the first time and attempted to figure it out.

The first experiment to determine the lifetime of the radical was done by Ortiz de Montellano and Stearns,^[3,12] using bicyclo[2.1.0]pentane (Scheme 1). Using the percentage of rearrangement [*U/R*] and the free-radical rearrangement rate constant, k_r , enabled them to quantitate the lifetime of the radical as 50 ps. However, since the products were exclusively the *endo* isomers, it was further concluded that the radical can rearrange but its reorientation, from the *endo* to the *exo* face, is restricted within the pocket of the protein. A similar conclusion was reached by Sligar et al.^[6] for the C–H hydroxylation of camphor by P450cam, by Jones et al.^[13] for C–H hydroxylation of *para*-xylene, and so on.^[3] By contrast, an NMR study by Ortiz de Montellano^[14] showed that a substrate like adamantane is mobile within the timescale of the enzymatic turnover within the pocket. It appears, therefore, that the restricted mobility of the radical is anisotropic. Other studies of radical clocks followed, and generated a variety of lifetime data, which indicated that the radicals are short-lived and somewhat restricted in their motions.^[3]

The support for the rebound mechanism looked solid until Newcomb et al.^[15–18] began their investigation of ultrafast radical clocks and carbocationic clocks. Thus, Newcomb has shown that the quantity [*U/R*] for a series of radical clocks does not correlate with the known lifetimes of the putative free-radical clocks.^[15] Some rearrangement patterns of clocks like **1**, depicted in Scheme 2, were shown to correspond to carbocationic species.^[16,18–20] Subtraction of these carbocationic rearrangements from the overall product mixture resulted in lifetimes as short as 70 fs;^[16,18] durations much too short to qualify as lifetimes of a real intermediate species. These unrealistic lifetimes and the rearranged products derived from carbocations have led Newcomb and co-workers^[15] to suggest that radical intermediates are not present during the reaction, and that alkane hydroxylation proceeds by two competing mechanisms nascent from two oxidant species of the enzyme, Cpd I and its precursor ferric peroxide species, so called Cpd 0 (Figure 1). As shown in Scheme 2, one mechanism involves a concerted [O] insertion from Cpd I into the C–H bond, while the second one involves hydroxonium ion (OH⁺) insertion from Cpd 0 into the C–H bond. This latter process generates a protonated alcohol, which subsequently rearranges in a manner typical of a carbocation, with no in-



Scheme 2. The two-oxidant hypothesis using Cpd I and Cpd 0, and a probe substrate (**1**) that can open differently depending on whether it leads to a radical or a cationic intermediate (ref.^[15])

termediary of free carbocations. Newcomb's work has cast the rebound mechanism into doubt and started what is dubbed in the title of this work, as “*the rebound controversy*”, which is still ongoing.^[20–22]

The “rebound controversy” touches the limits of chemistry's capabilities to pinpoint complex reaction mechanisms. Its importance derives from these limits, because it forces us to grapple with the state-of-the-art of our understanding of molecular processes. An eventual resolution of this controversy will no doubt come from the interplay of theory and experiment. Theory has already offered a resolution of the main elements in the controversy.^[23–26] Since then, a few more theoretical studies were performed by the Jerusalem group,^[27,28] and by Yoshizawa et al.^[29–31] Also relevant is the molecular dynamics simulations by Gualar et al.^[32] which described the rebound step in the enzyme methyl monooxygenase (MMO), and which is interesting to compare to the rebound in P450. These studies cover a range of systems and pose an opportunity to give an overview intended to refine our current understanding of the controversy, with a focus on the rebound step that appears to be the origin of the intriguing controversy.

Results and Discussion

Background: Theoretical Calculations of Alkane Hydroxylation and Key Points of Contention and Focus

In 1998, Shaik et al.^[23,33] offered a possible reconciliation of the controversy based on the two-state reactivity (TSR) paradigm. Subsequently, the Jerusalem group^[23,24,26,27] used density functional theory (DFT) to compute model alkane hydroxylation reactions between Cpd I (HS[−] as a proximal ligand) with methane and propene. As shown in the energy profiles in Figure 2, the computations reveal that alkane hydroxylation proceeds via two states, one is a high-spin (HS) quartet state and the other is a low-spin (LS) doublet state. These two states originate in the ground state of Cpd I that possesses three unpaired electrons, which give rise to two closely lying HS and LS states, separated in energy by a few wavenumbers.^[34–36] The reaction path involves a C–H activation phase, which looks like a hydrogen-abstraction process, leading to a radical, loosely coordinated to the iron–hydroxo intermediate by a C···HO hydrogen bond, followed by a reorientation phase in which the radical rotates away from the OH bond to form a direct C···O contact, and finally a rebound phase in which the radical attacks the oxygen atom to form the C–O bond of the alcohol.

The HS and LS profiles are close in energy, all the way to the PorFeOH/Alk⁺ cluster, and subsequently they bifurcate. In the LS manifold, once the radical snaps out of the C···HO hydrogen interaction with the iron–hydroxo species, the ensuing LS rebound phase is barrierless.^[23,24,27] By contrast, the HS rebound has a significant barrier to rebound, with a real transition state that has clear structural and spin density features, indicative of the source of activation. As such, the radical intermediate will have a suffic-

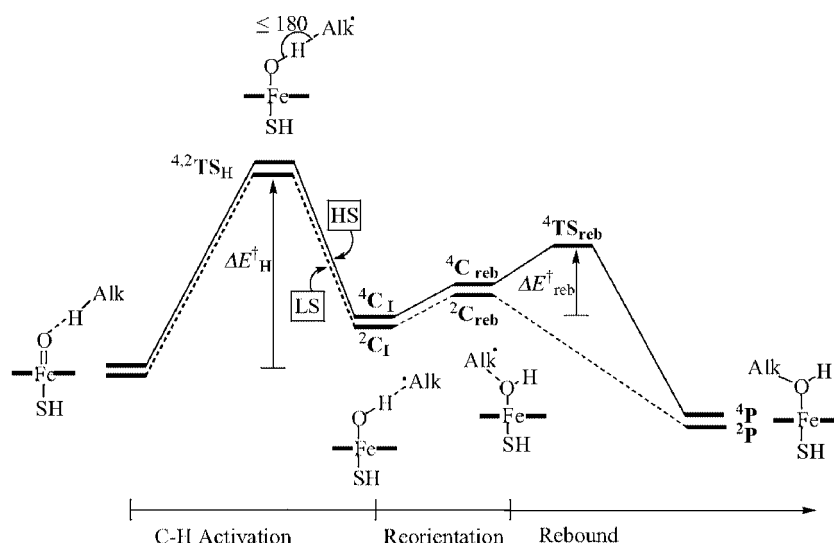


Figure 2. Reaction profile of alkane hydroxylation by Compound I, as calculated by density functional theory using porphine and L = SH[−]; note the doubling of the profile to high-spin (HS) and low-spin (LS) components

iently long lifetime on the HS manifold. By contrast, the lifetime of the LS intermediate will be shorter than the HS and its upper limit will be set by the frequency of rotational modes, which establish a rebound position. Thus, the “lifetime of the radical” in this scenario is a two-state information content with an ultrashort component and a “normal” longer component.

Extending this picture to a clock experiment (Scheme 1) means that the amount of rearranged product *R* originates mainly in the HS state, while the unrearranged product *U* is contributed by both HS and LS states, although mostly by the LS state. Thus, the apparent radical lifetime, which is quantified from the ratio [*U/R*], is not a true lifetime, since it reflects the relative yields of the HS and LS processes. At the limiting case when rearrangement occurs only on the HS manifold, the [*U/R*] quantity will be equal to the percentage of the LS and HS processes in the total product yield. As a rule, within the two-state picture, the quantity [*U/R*] will yield apparent lifetimes that are shorter than the real ones. Ultrashort apparent lifetimes will result whenever the contribution of HS processes to the total hydroxylation reaction is very small. This TSR explanation^[23,26] provided a reasonable solution of the controversy and revealed a scenario that, on the one hand, accommodated the KIE evidence, indicating a hydrogen-abstraction-like transition in the bond activation, and, on the other hand, demonstrated the reason for the controversial apparent lifetimes, which are determined assuming that the [*U/R*] quantity is a result of a single radical intermediate that is partitioned between instant rebound and rearrangement followed by rebound, as in Scheme 1.

Recent results of Newcomb et al.^[37,38] indicate that the ratio [*U/R*] is subject to an isotope effect when the hydrogen atom is replaced by a deuterium atom in the scissile C–H bond. This finding of a product isotope effect rules out a single pathway or a single intermediate that is partitioned between rebound and rearrangement pathways. The ob-

served product isotope effect can therefore indicate the operation of either TSR or two-oxidant (Scheme 2) scenarios. However, recent calculations by the Jerusalem group showed that Cpd 0 has a very high barrier for olefin epoxidation (its marker reaction), much higher than that which is calculated with Cpd I as an oxidant.^[39] More recent DFT calculations^[40] show the same trend for sulfoxidations, for which the barrier is much higher than with Cpd I, even when Cpd 0 is assisted by a powerful proton source. Thus, *DFT calculations rule out the possibility that Cpd 0 can compete with Cpd I as an oxidant.* Furthermore, the cryogenic EPR and ENDOR experiments of Davydov et al.^[41] for camphor hydroxylation support oxidation by Cpd I, but not by Cpd 0. Even the most recent experimental evidence, which implies that Cpd 0 can indeed epoxidize olefins, shows that the putative reaction is sluggish compared with that of Cpd I and occurs only in the absence of Cpd I.^[42] Similarly, radical-derived rearrangements were produced from model systems which involve only Cpd I as an electrophilic oxidant.^[43,44] Thus, while one cannot rule out the presence of another oxidant, in the absence of Cpd I, at this stage of the research, the balance seems to favor the TSR scenario with only Cpd I as a plausible mechanism of hydroxylation by P450.^[3]

Two DFT studies of ethane hydroxylation were performed by Yoshizawa et al.^[29,30] using a model Cpd I with MeS[−] as a proximal ligand. Their two studies indeed revealed TSR with bond-activation transition states that look like hydrogen-abstraction species. However, there were conflicting results and differences with the results of Ogliaro et al.^[23,45] Thus, the study with the better basis set^[29] reveals an HS profile that is ca. 6 kcal·mol^{−1} lower than the LS profile, while with a smaller basis set,^[30] the HS–LS energy differences are small (0.6–3.2 kcal·mol^{−1}), but the HS profile is higher than the LS, in agreement with the results of Ogliaro et al.^[23] The most recent study of camphor hydroxylation, by Kamachi and Yoshizawa,^[31] which used a large

basis set, gave a difference of $2.2 \text{ kcal}\cdot\text{mol}^{-1}$ between **HS** and **LS** barriers, in somewhat better agreement with Ogliaro et al.^[23,45] but still the lower profile is that of the **HS** process. We think that these switches in the results originate in the choice of the thiolate ligand to model the cysteinate ligand within the protein pocket. In a recent quantum mechanical/molecular mechanical (QM/MM) study, Schöneboom et al.^[46] showed that Cpd I, with MeS^- as a proximal ligand, exhibits a greater sensitivity to basis set and environmental effects, than with the model HS^- as a proximal ligand. Furthermore, it was shown that with HS^- , the gas-phase calculation of Cpd I is closer to its final state in the protein pocket.

As far as the rebound step is concerned, the earlier results of the Yoshizawa group^[29,30] were in conflict with those of Ogliaro et al.,^[23] although the most recent ones appear to be in good agreement. Thus, the DFT calculations of camphor hydroxylation by Kamachi and Yoshizawa,^[31] with a good-quality basis set, led to a picture similar to that which was obtained by Ogliaro et al.,^[23] with an **LS** rebound that has a very tiny barrier, $0.7 \text{ kcal}\cdot\text{mol}^{-1}$, and an **HS** rebound that has a substantial barrier of more than $3 \text{ kcal}\cdot\text{mol}^{-1}$. Even though the remaining disagreements are minimal, nevertheless these apparently conflicting results highlight both the complexity of the rebound process as well as *the need for a fundamental theoretical understanding of the rebound problem*, rather than over-reliance on computations alone. Thus, since there is an experimental and theoretical consensus about the nature of the bond-activation step, the remaining doubts concern the rebound step. As such, the major questions, which are addressed in this Microreview are the following: *What is the origin of the HS rebound barrier? Why does the LS process have a tiny rebound barrier, if at all? Will the LS rebound barrier always be tiny?*

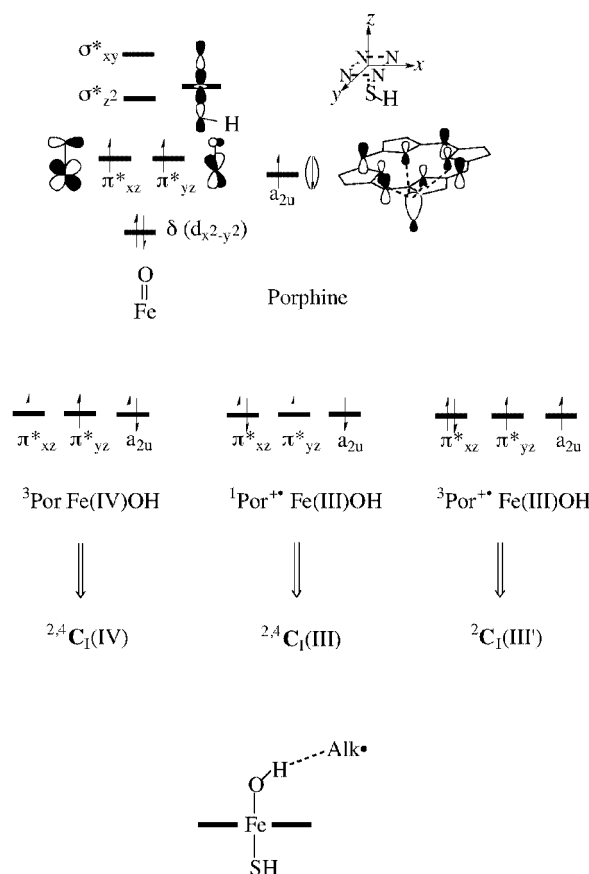
There are several issues within these questions. One issue concerns the electromeric identity of the iron–hydroxo intermediate, which can either be a ferric, $\text{Por}^{+\cdot}\text{Fe}^{\text{III}}\text{OH}$, species or a ferryl, $\text{PorFe}^{\text{IV}}\text{OH}$, one. In an early paper^[47] the Jerusalem group argued that in the protein pocket the ground states of the iron–hydroxo complex will be the $\text{Por}^{+\cdot}\text{Fe}^{\text{III}}\text{OH}$ species. Accordingly, the studies of Harris et al.^[24] and Ogliaro et al.^[23] described the rebound processes for $\text{Por}^{+\cdot}\text{Fe}^{\text{III}}\text{OH}/\text{Alk}'$, but pointed out that smaller barriers are expected for $\text{PorFe}^{\text{IV}}\text{OH}/\text{Alk}'$ ($\text{Alk}' = \text{methyl, allyl}$). Recent EXAFS studies of the iron–hydroxo species of the enzyme chloroperoxidase indicate that the ground state is $\text{PorFe}^{\text{IV}}\text{OH}$,^[48] and similar results were obtained computationally.^[27,47,49] However, the results of Groves et al.^[50] and Gross et al.^[51] show that in model systems in solution, both electromers may coexist. Therefore, in the following sections, we address the question of the ground state of the iron–hydroxo species, and the respective rebound barriers of the ferric and ferryl states.

The second issue is the behavior of the **HS** vis-à-vis the **LS** rebound step. We now have data on rebound processes in methane,^[23] camphor^[31,52] and propene^[27,49] hydroxylations, and in epoxidations of ethene^[25] and propene,^[27,49] as well as in methane hydroxylation by a ruthenium analog

of Cpd I.^[28] Based on this insight, we shall present a valence-bond model for the rebound process on the **HS** and **LS** states. Using this model we shall attempt to pattern the existing experimental data of radical scrambling during alkane hydroxylation. Finally, we shall assess the possible sources of carbocations, which are implicated by the studies of Newcomb and co-workers^[15,20] and the recent studies of Ortiz de Montellano and Groves et al.^[21]

Electromeric States of the Iron–Hydroxo Species and the Iron–Hydroxo/Alk' Cluster Intermediate

The iron–hydroxo intermediate formed in the hydrogen abstraction step of Figure 2 possesses three low-lying states, shown in Scheme 3, using the d-block and other key orbitals. These are the π^* -orbitals [antibonding $d_{xz,yz}(\text{Fe})$ - $p_{x,y}(\text{O})$ combinations], and the a_{2u} orbital [an antibonding $a_{2u}(\text{Por})$ - $p_z(\text{S})$ combination]. Other orbitals are the δ -orbital on the iron atom, which is always doubly occupied, and the $d_z^2(\sigma_z^2)$ orbital, which becomes populated during the **HS** rebound process. The ferryl state involves two singly occupied π^* -orbitals, which, together with the doubly occupied δ -orbital, correspond to a d^4 metal configuration, and hence to the $^3\text{PorFe}^{\text{IV}}\text{OH}$ electromer. The other two states involve singly occupied π^*_{yz} and a_{2u} , which, together with



Scheme 3. An orbital diagram showing the occupancy in the ferryl(IV) electromer of the iron–hydroxo complex; below are the occupancies of the lowest electromeric species, Fe^{IV} and Fe^{III} , of this complex, along with their corresponding occupancies; the spin-state assignments are indicated by the superscripts

the double occupancy of δ and π^*_{xz} correspond to a d^5 metal configuration and a radical cation situation formally on the porphyrin, hence the $^{1,3}\text{Por}^+\text{Fe}^{\text{III}}\text{OH}$ electromer states. Addition now of the alkyl radical gives rise to five different states of the iron–hydroxo/Alk' cluster, labeled as $^{2,4}\text{C}_1(\text{IV})$, $^{2,4}\text{C}_1(\text{III})$ and $^{2,4}\text{C}_1(\text{III}')$.

The geometries and spin densities of the ferryl and ferric varieties are depicted in Figure 3a for the simple model with porphine and HS^- as proximal ligand. All values in parentheses refer to a polarizing environment, characterized by a dielectric constant, ϵ , of 5.7. The ferric species exhibits greater sensitivity to the polarizing environment. Thus, reminiscent of our findings for Cpd I,^[46,52,53] the $\text{Por}^+\text{Fe}^{\text{III}}\text{OH}$ species undergoes Fe–S bond shortening and charge transfer from the porphyrin to the sulfur atom. By contrast, the ferryl species, $\text{PorFe}^{\text{IV}}\text{OH}$, is less sensitive to the environmental effect. The relative ordering of the ferric and ferryl species depends on a few variables (see detailed data in the Supporting Information) and can be described as follows. With the double-zeta LACVP(6-31G) basis set, the ground state of the bare system is the ferryl species. A larger basis set, LACV3P+*(6-311+G*), increases this preference to 5.2 kcal·mol⁻¹. Medium polarization and geometry optimization, however, stabilize the ferric states relative to the ferryl ones and decrease the difference to 3.14 kcal·mol⁻¹, as indicated in Figure 3a.

A more extensive model is the species with octamethylporphyrin and the full cysteinato ligand, shown in Fig-

ure 3b, with LACVP(6-31G) geometric values, alongside the energy differences obtained by single-point calculations with the triple-zeta LACV3P basis set and with inclusion of medium polarization. The energy difference of 1.72 kcal·mol⁻¹ in favor of the ferryl situation is the highest limit of this difference. An estimate of the energy difference due to the effect of geometry optimization leads to a smaller difference of less than 0.7 kcal·mol⁻¹ (values in parentheses). One can further expect that the real protoporphyrin substituents, two vinyl groups and two propionate anions, may tip the balance.^[47]

Bringing in the alkyl radicals will give rise to the five states of the $\text{PorFeOH/Alk}'$ intermediate en route to the rebound step (see Scheme 3). The interaction of the alkyl group with the iron–hydroxo is by means of an $\text{H}\cdots\text{C}$ hydrogen-bonding interaction of the $\text{FeOH}\cdots\text{C}(\text{Alk}')$ type, which leads to the intermediates $^{2,4}\text{C}_1$ in Scheme 3. Since the carbon atom of the alkyl group is slightly negative and the hydrogen atom of the hydroxo group is slightly positive, this hydrogen-bonding interaction will further modulate the energy differences between the ferric and ferryl states. The calculations show that the ferryl complex has a slightly larger positive charge on the hydrogen atom than in the ferric state, and therefore one might expect that the preference for the ferryl intermediate will be slightly larger in the presence of the radical, as is indeed borne out by all the calculations. However, this interaction is expected to be undermined in the presence of the screening effect of the

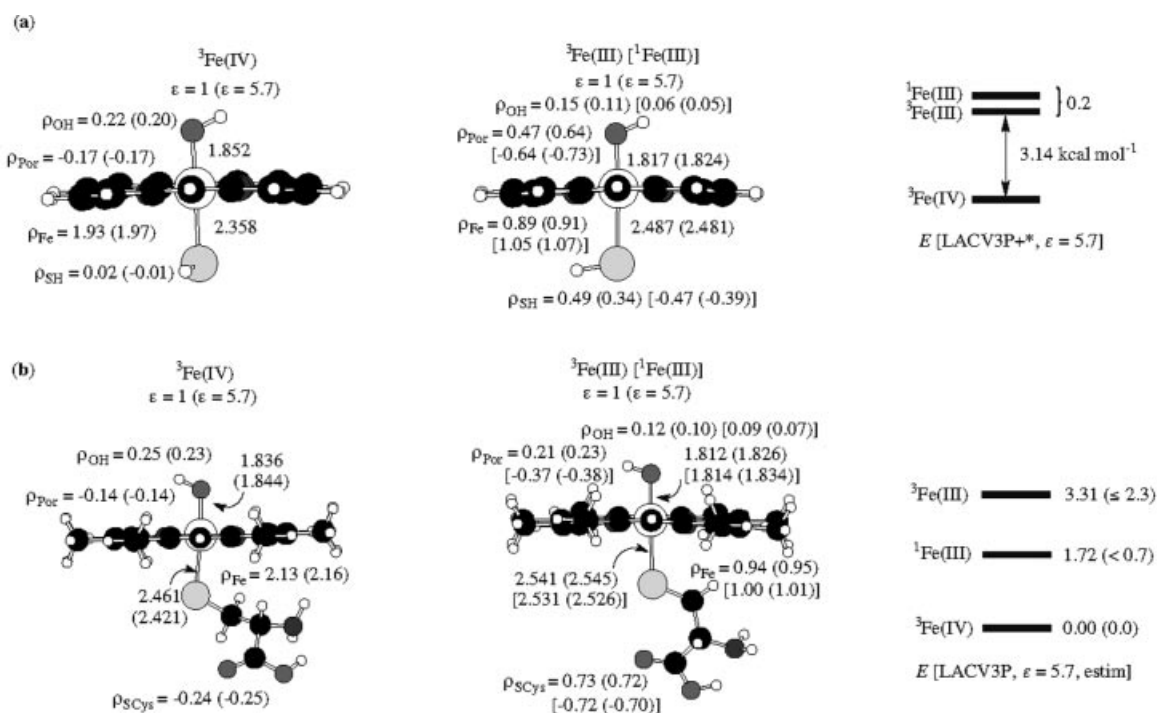


Figure 3. (a) B3LYP/LACVP geometries of the iron–hydroxo complex, using porphine and $\text{L} = \text{SH}^-$; the spin densities (ρ) are taken from a single point calculation with the LACV3P+* basis set in vacuo and in a dielectric medium with $\epsilon = 5.7$; the diagram on the right shows relative energies calculated with the LACV3P+* basis set and in a dielectric medium with $\epsilon = 5.7$; (b) B3LYP/LACVP geometries for the electromeric species of the iron–hydroxo complex, using octamethylporphyrin and $\text{L} = \text{cysteinate}$; structures were fully optimized in vacuo and in a solvent with a dielectric constant of $\epsilon = 5.7$; the spin-density values are taken from single-point calculations with the LACV3P basis set; the diagram on the right shows relative energies calculated using the single point energies with LACV3P and in a dielectric medium with $\epsilon = 5.7$; the values in parentheses are estimated relative energies corrected for the effect of geometry optimization

protein pocket. The resulting clusters from our most recent QM/MM study of camphor hydroxylation by P450cam are depicted in Figure 4. The group spin densities clearly illustrate that, under a realistic representation of the protein environment, the ferric electromers are the ground states, but the ferryl states lie very close in energy,^[52] as is indeed shown by experiment for model systems in chlorinated solvents.^[50,51] Since, for realistic alkanes, all the five intermediate states will lie below the hydrogen abstraction transition states, $^2,4\text{TS}_\text{H}$ (Figure 2), in principle, they will all be accessible for rebound, and may further complicate the TSR picture into a multi-state scenario, where both spin and oxidation states are variable.

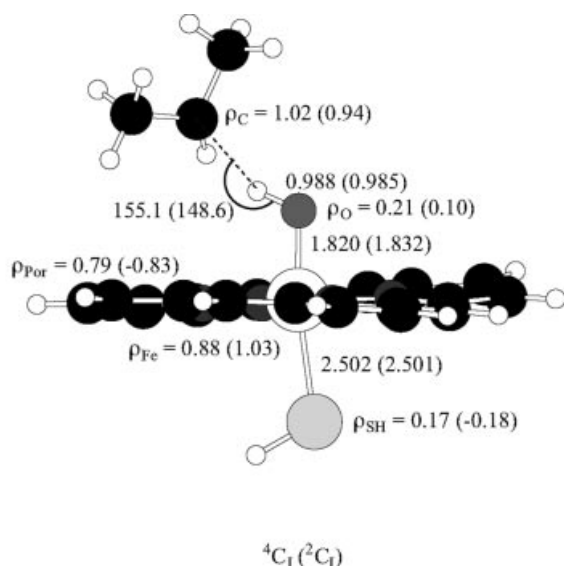
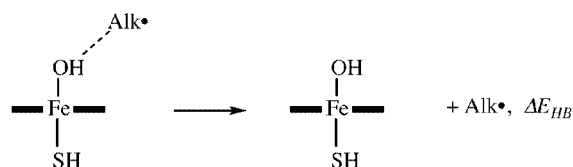


Figure 4. A QM/MM snapshot showing only the QM subsystem of the $^2,4\text{C}_1(\text{III})$ clusters for camphor (truncated in the figure) hydroxylation by P450cam (ref.^[52]); key geometric features and group spin densities (ρ) are indicated near the corresponding moieties; the LS cluster is 1.08 kcal/mol lower than the HS cluster

Is the Radical Free, Bound or a “Guided Radical”?

The computational data in Scheme 4 show that the strength of the $\text{FeOH}\cdots\text{C}(\text{Alk}^\bullet)$ hydrogen bond in C_1 is of the order of 1.9–2.7 kcal·mol^{−1}, and is marginally dependent on the radical, methyl vis-à-vis allyl. The weakness of this interaction is manifested in the presence of six-to-nine modes of very low frequencies, less than 100 cm^{−1}, and a few others with less than 200 cm^{−1}, which describe the relative movement of the alkyl radical with respect to the iron–hydroxo species, for example, $\omega = 81.9 \text{ cm}^{-1}$ for the stretching mode of the hydrogen bond, $\text{H}\cdots\text{CH}_3$. These frequencies are collected in the Supporting Information for the cases of methyl and allyl radicals in the ferryl states. Some of these modes are internal rotations of the radical, while others involve what may look like a stretching mode of the $\text{H}\cdots\text{C}$ hydrogen bond, and still others look like reorientation modes, which converts the C_1 cluster to a C_H cluster held by a $\text{C}-\text{H}\cdots\text{OFe}$ hydrogen bond, as well as swing and flip modes. For example, a swing motion that changes the

terminal of the allyl radical that is coordinated by the $\text{FeOH}\cdots\text{C}$ hydrogen bond, will be responsible for allylic scrambling. Likewise, a flip of the radical (self rotation), which changes the face that is coordinated to the iron–hydroxo species, will be responsible for inversion of configuration of the radical. Clearly, therefore, the radical is loosely coordinated and has a great deal of freedom at a small energy expense.



Alk	Fe	ΔE_{HB} (kcal mol ^{−1})
CH_3	Fe(III)	1.9 (HS); 2.1 (LS)
CH_3	Fe(IV)	2.6 (HS); 2.7 (LS)
C_3H_5	Fe(III)	not available
C_3H_5	Fe(IV)	2.3 (HS); 2.7 (LS)

Scheme 4. $\text{OH}\cdots\text{C}$ hydrogen bonding energies (ΔE_{HB}) calculated at the B3LYP/LACVP level

Is the radical “bound” or is it a free radical? Since the interaction is rather small and since coordination causes the fragments to lose their individual rotational entropies ($T\Delta S \approx -6 \text{ kcal}\cdot\text{mol}^{-1}$), on the free-energy scale the separated fragments are more abundant than the $\text{FeOH}\cdots\text{C}(\text{Alk}^\bullet)$ cluster, i.e., *there are more radicals that are not bound to the iron–hydroxo complex than radicals that are*. The portion of the bound species^[32,54,55] will perform a periodic motion along the $\text{C}\cdots\text{H}$ hydrogen-bonding coordinate, as recently described in the semi-classical trajectory study of the rebound step in the enzyme MMO.^[32] However, all this may be less relevant since a major consideration should be given to the situation in the protein pocket. Substrate binding by the protein is different for different P450 isozymes.^[21] For example, in the enzyme P450_{cam}, the side chain Tyr96 holds the camphor by a hydrogen bond, $\text{C}=\text{O}\cdots\text{HO}-\text{Tyr}$, to its carbonyl group.^[56] This hydrogen-bonding interaction is quite exergonic, in part because it is *entropically driven* by the release of a few water molecules. Thus, this interaction appears to be more important than the weak $\text{FeOH}\cdots\text{C}(\text{Alk}^\bullet)$ hydrogen bond between the alkyl group and the iron–hydroxo species. This hydrogen bonding to Tyr96 continues to hold the camphoryl radical and may even serve to reorient it towards a favorable rebound position. Thus, *we might be dealing with a “guided radical” that is conveniently oriented to the rebound position by the protein*. These protein-binding modes must be taken into account in a molecular dynamics study, and these may over-

shadow the weak interaction found in the gas-phase calculations. Until such time when a molecular dynamics study within the protein can be conducted, we limit the analysis of the rebound step to a few essential features, which depend on clear electronic factors.

The Reorientation and Rebound Phases

Among the low-frequency vibrations of 2,4C_1 , a unique mode is the one that involves either rotation of the alkyl group around the $O\cdots C$ axis, or the one in which the rotation of the radical is coupled to the $O-H$ rotation around the $Fe-O$ axis. Both movements bring the radical to the backside of the $H-O$ bond to the rebound position (see Figure 2). This motion, which leads to the release of the radical from the $FeOH\cdots C(Alk')$ hydrogen bond, involves an energy rise of the order of $1-1.5\text{ kcal}\cdot\text{mol}^{-1}$. Both the **HS** and **LS** $FeOH\cdots C(Alk')$ species possess this feature.^[23] However, once the radical snaps out of this interaction and maintains a "rebound position" with a direct $O\cdots C$ orientation, the **LS** and **HS** rebound processes differ in a fundamental manner. The **HS** rebound has an additional "chemical" barrier to surmount with a distinct transition state,^[23,24,27] whereas the **LS** rebound is barrier-free. This, at least, is the situation in the alkyl radicals tested so far.

Table 1 collects the **HS** rebound barriers, $\Delta E_{\text{reb}}^\ddagger$, for the various systems studied in our group and others, including for epoxidation. These barriers are seen to be significant and to depend on the oxidation state of the iron atom in the iron-hydroxo complex [$\Delta E_{\text{reb}}^\ddagger(\text{III}) > \Delta E_{\text{reb}}^\ddagger(\text{IV})$], on the identity of the transition metal [$\Delta E_{\text{reb}}^\ddagger(\text{Fe}) \ll \Delta E_{\text{reb}}^\ddagger(\text{Ru})$], as well as on the proximal ligand [$\Delta E_{\text{reb}}^\ddagger(\text{SH}^-) > \Delta E_{\text{reb}}^\ddagger(\text{MeSO}_3^-) \geq \Delta E_{\text{reb}}^\ddagger(\text{ImH})$]. A polarizing field (mim-

icked by a dielectric constant, ϵ , of 5.7) raises the barrier for the Fe^{III} electromer by a significant amount, ca. $4-5\text{ kcal}\cdot\text{mol}^{-1}$, but the effect on the Fe^{IV} electromer is small and is counteracted by the effect of $NH\cdots S$ hydrogen bonding and further lowered by inclusion of zero-point energy effect (ZPE). As such, for the Fe^{IV} electromer, the calculated gas-phase barrier is a good approximation for the barrier that includes all these effects, while for the Fe^{III} electromer the barrier is significantly raised by the polarity of the medium.

A few rebound transition states, ${}^4TS_{\text{reb}}$, are depicted in Figure 5, along with a typical example of the reaction vector (the mode with imaginary frequency), which shows a clear rebound mode. The geometries of the ${}^4TS_{\text{reb}}$ species exhibit $Fe-S$ and $Fe-O$ bond elongation vis-à-vis their corresponding 4C_1 clusters. Finally, all the ${}^4TS_{\text{reb}}$ species exhibit reduction of the spin density on the radical and increase of the spin densities on iron, while the ${}^4TS_{\text{reb-III}}$ species exhibit, in addition, depletion of the spin density on the porphine. Thus, both geometric as well as electronic changes accompany the **HS** rebound process.

In contrast to the **HS** rebound, once the radical in the **LS** intermediate assumes a rebound position, the ensuing rebound proceeds in a barrierless fashion for both ferryl and ferric states (Figure 2).^[24,27] An illustrative example of the **LS** rebound is the behavior of ${}^2\text{PorFe}^{IV}\text{OH}/\text{allyl}'$ shown in Figure 6. During the $C\cdots O$ shortening, the allyl radical swings around the $Fe-O$ bond to a rebound position, the energy rises by about $1.5\text{ kcal}\cdot\text{mol}^{-1}$ and then falls abruptly to the product complex, 2P . The top structure of the potential energy profile always falls back into ${}^2C_1(\text{IV})$ upon transition-state-optimization procedures. A frequency calcu-

Table 1. High-spin (HS) rebound barriers from the 4C_1 clusters

Entry ^[a]	4C_1 species	Radical	${}^4\Delta E_{\text{reb}}^\ddagger$ ^[b]	${}^4\Delta E_{\text{reb}}^\ddagger(\text{ZPE})$ ^[b]	${}^4\Delta E_{\text{reb}}^\ddagger(\epsilon = 5.7)$	${}^4\Delta E_{\text{reb}}^\ddagger(2NH\cdots S)$
a) Hydroxylation						
1	$C_1(\text{III})$	CH_3	4.9 (5.5)	—	9.8	—
2	$C_1(\text{IV})$	CH_3	3.3 (3.4)	2.9 (3.0)	4.9	—
3	$C_1(\text{IV})$, Ru	CH_3	12.6	—	—	—
4	$C_1(\text{IV})$	C_3H_5	3.9 (3.7)	(3.4)	5.2	2.5
5	$C_1(\text{III})$	C_3H_5	> 3.9	—	—	—
6	$C_1(\text{IV})$	$\text{C}_{10}\text{H}_{15}\text{O}$	3.3 ^[c]	—	—	—
7	$C_1(\text{III})$	$\text{C}_{10}\text{H}_{15}\text{O}$	> 9.7 ^[d]	—	—	—
8	$C_1(\text{IV})$, L = ImH	C_3H_5	(1.3) ^[e]	(0.7)	—	—
9	$C_1(\text{IV})$, L = MeSO_3^-	C_3H_5	1.9 ^[f]	(1.5)	—	—
b) Epoxidation						
10	$C_1(\text{IV})$	$\text{Fe}-\text{O}-\text{CH}_2\text{CH}_2\cdot$	2.3	—	—	—
11	$C_1(\text{III})$	$\text{Fe}-\text{O}-\text{CH}_2\text{CH}_2\cdot$	7.2	—	—	—
12	$C_1(\text{IV})$	$\text{Fe}-\text{O}-\text{CH}_2\text{CH}(\text{CH}_3)\cdot$	0.7 (0.9)	(0.3)	(0.6)	2.6
13	$C_1(\text{III})$	$\text{Fe}-\text{O}-\text{CH}_2\text{CH}(\text{CH}_3)\cdot$	> 9	—	—	—

^[a] In kcal/mol. Unless indicated otherwise, the proximal ligand L is thiolate, SH^- , and the transition metal is iron, Fe. All calculations refer to B3LYP/LACVP. ^[b] Energy values calculated with Jaguar. Energy values in parentheses calculated with Gaussian 98. ^[c] Camphor rebound barrier in the gas phase from ref.^[31] ^[d] Estimated energy barrier of camphoryl rebound in the enzyme P450cam as calculated by QM/MM (value taken from the highest point in the scan, from ref.^[52]). ^[e] Unpublished results using Cpd I model of HRP. ^[f] Unpublished results using Cpd I model of Woggon's reagent.

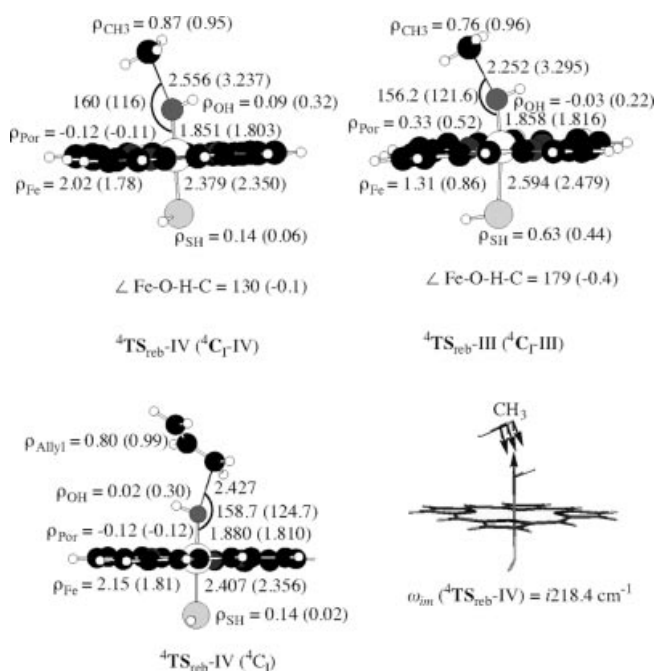


Figure 5. Rebound transition states for the **HS** process, ${}^4\text{TS}_{\text{reb}}$, with key geometric values and spin densities (ρ); the right-hand bottom drawing exemplifies the reaction vector (imaginary mode) for the methyl rebound ${}^4\text{TS}_{\text{reb}}$ species of the Fe^{IV} electromer

lation on this top structure revealed the imaginary mode displayed in the figure. It can be seen that this mode has no rebound component and is a pure rotational motion that connects the $\text{OH}\cdots\text{C}$ -coordinated ${}^2\text{C}_1(\text{IV})$ conformer to the rebound conformer by a direct $\text{C}\cdots\text{O}$ contact. Since the latter conformer is not a real minimum, nor a saddle point, it falls abruptly to the alcohol complex product. Such rotational structures were found also for the ${}^2\text{C}_1(\text{IV})$ intermediate of methyl radical where the imaginary rotational mode ($\omega = i92.4\text{ cm}^{-1}$) involved coupled rotation of the OH group and the methyl radical (see Supporting Information). Similar results were reported by Kamachi and Yoshizawa,^[31] who located an **LS** rebound transition state with a purely rotational reaction vector ($\omega = i29.4\text{ cm}^{-1}$). The orientational nature of these structures is further evident by noting that they involve very little, if any, change in structure and spin-density distribution compared to the ${}^2\text{C}_1(\text{IV})$ intermediate (see ρ and bond lengths in Figure 6). All the ${}^2\text{C}_1(\text{III})$ intermediates for both allyl and methyl radicals either fell down to the corresponding alcohol products, or exhibited featureless rotational profiles en route to the products, ${}^2\text{P}$, with structures having two or three imaginary modes corresponding to internal rotations within the cluster. Qualitatively identical results were found in our QM/MM study of the rebound process.^[52]

It follows that the weak $\text{FeOH}\cdots\text{C}(\text{Alk}')$ hydrogen bond forms a flat rotational ridge that separates the **LS** iron-hydroxo/(Alk') intermediate and the product alcohol complex. Once the alkyl radical snaps out of this interaction, the rebound itself is a continuous downhill process. These orientational barriers amount to $0.3\text{--}1.5\text{ kcal}\cdot\text{mol}^{-1}$

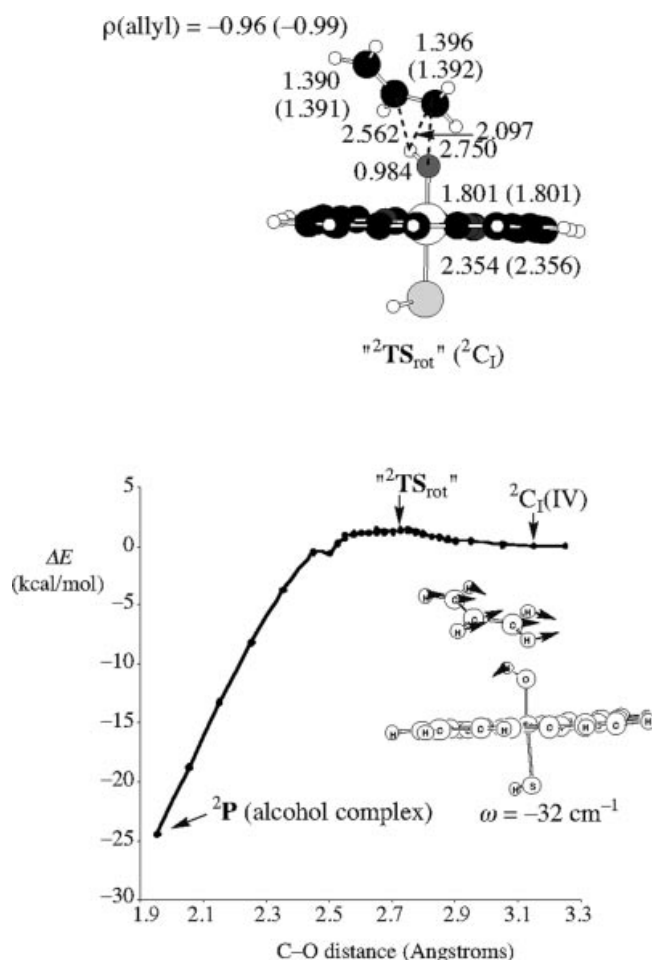


Figure 6. Illustration of the energy profile for an **LS** rebound process of the allyl radical; the topmost structure, ${}^n2\text{TS}_{\text{rot}}$, corresponds to a coupled rotation of the allyl radical and the OH group to assume a rebound position with a direct $\text{C}\cdots\text{O}$ contact; the arrows indicating the imaginary mode of ${}^n2\text{TS}_{\text{rot}}$ illustrate this coupled rotation; the structures on top correspond to the ${}^n2\text{TS}_{\text{rot}}$ species and to its precursor cluster, ${}^2\text{C}_1$; note the virtual identity in the geometric features, and in the spin densities (ρ) of ${}^n2\text{TS}_{\text{rot}}$ and ${}^2\text{C}_1$

for the various systems studied in our group. This analysis of the **LS** rebound is supported nicely by the results of the **LS** rebound in olefin epoxidation, where the radicals are not coordinated by hydrogen bonding to the iron-oxo complex and have barrierless rebound processes.^[25,27] In conclusion, therefore, the barriers for **HS** rebound will be significantly higher than those for the **LS** rebound. Accordingly, we may expect that the lifetime of the radical on the **LS** surface will be much shorter than on the **HS** surface, and be limited by the rotational mode that the alkyl group (or OH) has to perform to establish rebound position.

The question is: Will the radical on the **LS** surface have sufficient lifetime to rearrange, or will the entire **LS** hydroxylation process be effectively concerted, while all the rearranged products will be originating in the **HS** process? In P450 hydroxylation, the rebound barriers on the **HS** surface are of the order of $\geq 4\text{ kcal}\cdot\text{mol}^{-1}$ (Table 1), and are larger for the ferric states, ${}^4\text{C}_1(\text{III})$, and within a polarizing en-

environment. These **HS** rebound barriers are larger than, or of the order of, the barriers for skeletal rearrangements of radicals,^[57] for face-flip modes leading to inversion of chirality in the product, and for a heme alkylation process.^[58] By contrast, these barriers are much larger than the ones for positional swing modes, such as migration of allylic groups that leads to allylic scrambling.^[27,59] *As such, we may anticipate that the **HS** pathway will give rise to anisotropical scrambling of the stereochemical information*, in a manner that depends on the barriers for the various rearrangement modes vis-à-vis the rebound barrier, as well as on the protein environment, which restricts some modes more than others. By contrast, the reorientational barriers on the **LS** surface, about 0.3–1.5 kcal·mol^{−1}, are smaller than the barriers for skeletal rearrangement in typical clocks. In this sense, the **LS** rebound will be effectively concerted. The only rearrangement modes that may compete with the **LS** rebound are softer ones (e.g., swing), which radical clocks may be able to perform, provided no restrictions exist in the protein pocket (see ref.^[21] for a similar discussion).

Finally, any quantitation of the rearrangement problem is based on the assumption that the rate of radical rearrangement in the clusters, ⁴C₁, is roughly the same as that of the free radicals. Recent B3LYP/LANL2DZ(6-31G*) results by Clark^[60] show that the barrier for rearrangement of the cyclopropylcarbinyl radical complexed to metal ions is about 1 kcal·mol^{−1} higher than the barrier for the free-radical rearrangement. Our own results for *trans*-phenylcyclopropylcarbinyl radical show that the rearrangements for the free radical have slightly (0.6 kcal·mol^{−1}) higher barriers than the coordinated ones.^[61] These results indicate that the coordination of the radical does not dramatically change its rearrangement rate. What may change it, how-

ever, are the constraints within the protein pocket. But as yet there is no such hard evidence that can contest the assumption behind the clock experiments, namely, that the rate of rearrangement of the clock can be approximated by those of the free-radical rearrangement data.^[15–19]

Origins of the Differences between LS and HS Rebounds

The difference between the **HS** and **LS** rebound processes has a fundamental origin. This can be appreciated by appeal to Figure 7, which depicts in part (a) the electronic structural changes attending the rebound processes of the ferryl ^{4,2}C_{reb}(IV) species to the respective alcohol complexes, ^{4,2}P. During these transformations, the iron center is enriched by one electron, Fe^{IV} → Fe^{III}. At the same time the Alk(C)···O linkage loses one electron and becomes a standard two-electron C–O bond. Starting from ^{4,2}C_{reb}(III) in part (b), the porphyrin radical cation gains the electron that is lost from the C···O linkage. Thus, during rebound, *the C–O bond formation is attended by a single electron shift formally from the alkyl radical to the heme moiety*. This is common to both **LS** and **HS**. However, while in the **LS** process the electron is shifted to the low-lying orbitals (π*_{xz} and a_{2u}), in the **HS** rebound the electron is shifted to the high-lying σ*(d_z²) orbital in order to conserve the quartet spin.

As illustrative examples, we show in Figure 8 the spin-density variation along the methyl rebound path of the ferric cluster for the **HS** and **LS** states. In both states, the free spins on the methyl and porphyrin moiety diminish; however, while in the **LS** state the spin on the iron atom does not vary much, in the **HS** state the spin on the iron atom increases from an initial value of unity to about 2.5 at the end of the rebound. Therefore, relative to the **LS** rebound, the **HS** process involves an additional electronic

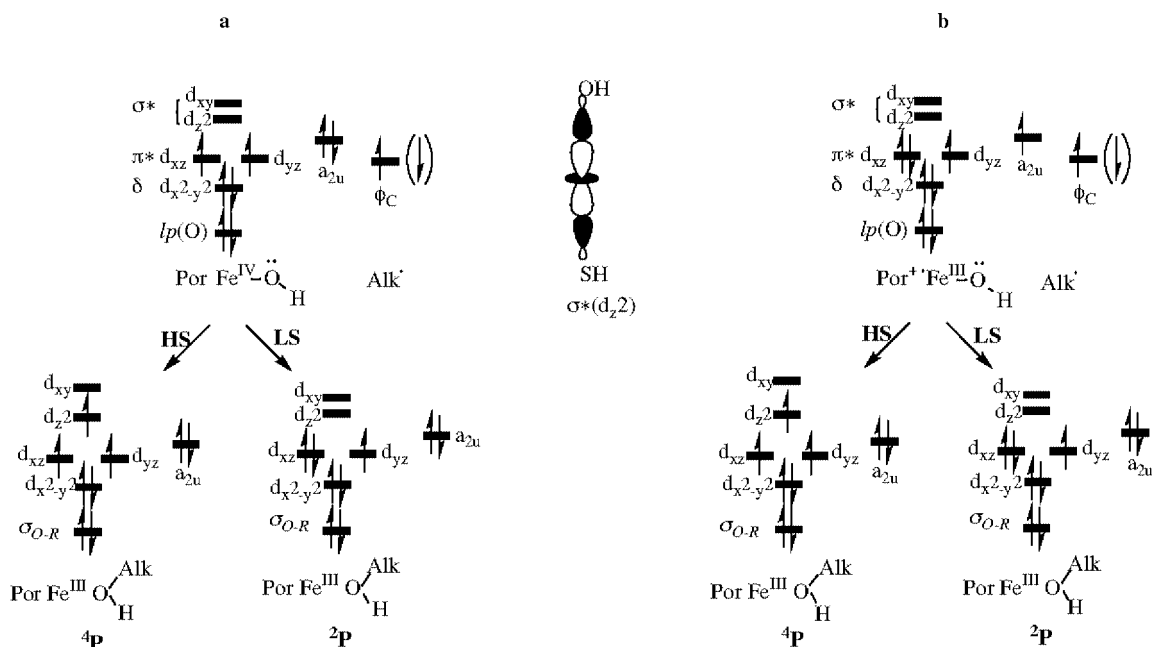


Figure 7. Orbital diagrams showing the electronic changes during rebound: (a) for the ferryl species, ^{4,2}C₁(IV), and (b) for the ferric species, ^{4,2}C₁(III); the σ*(d_z²) orbital is drawn in between the diagrams

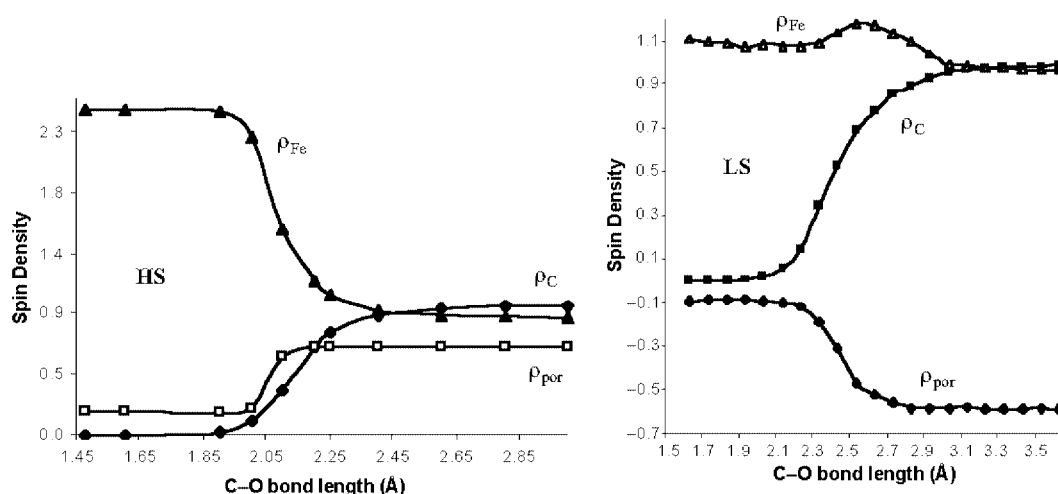


Figure 8. Spin-density (ρ) variation along the HS and LS rebound steps in methane hydroxylation; ρ_C corresponds to the spin on the methyl group, ρ_{por} on the porphyrin and ρ_{Fe} on the iron atom

excitation within the d-block orbital.^[23–25] This additional promotion to the $\sigma^*(d_z^2)$ orbital, which is antibonding in the S–Fe–O axis (Figure 7), is responsible for the lengthening of both Fe–S and Fe–O bonds in the $^4\text{TS}_{\text{reb}}$ species in Figure 5, and for the increase of the spin density on the iron atom and its decrease on the porphyrin in Figure 8. In turn, the lengthening of the Fe–O and Fe–S bonds is responsible for the HS rebound barrier. The role of the $d_z^2(\sigma^*)$ orbital is apparent by looking at the angle $\angle\text{FeO–C(Alk)}$ in the $^4\text{TS}_{\text{reb}}$ species (Figure 5). This angle is very wide, ca. 156° – 160° , compared with the much smaller angle in the corresponding clusters, and it thereby indicates that the accepting orbital is $\sigma^*(d_z^2)$ that lies along the Fe–O axis (see orbital depiction in Figure 7).

In contrast with the HS process, the LS rebound does not require this electronic promotion. As such, during the LS rebound the Fe–S undergoes shortening and becomes strengthened; for example, in the case of allyl radical LS rebound, the Fe–S bond is shortened by about 0.2 \AA for the various $^2\text{C}_1(\text{III,IV})$ situations.^[23,27] Part of this bond shortening is no doubt responsible for the fact that the LS rebound is considerably more exothermic (Figure 2) than the HS rebound, by ca. $7\text{ kcal}\cdot\text{mol}^{-1}$ (for methyl) and $13\text{ kcal}\cdot\text{mol}^{-1}$ (for allyl). Thus, the Fe–S bond shortening mitigates the energy rise due to the Fe–O bond lengthening and evidently eliminates altogether the rebound barrier in the LS manifold.

A Valence Bond (VB) Modeling of the Barrier for the Rebound Process

To outline a systematic structure-reactivity relationship for the rebound process, we present here a valence bond (VB) analysis of the origins of the barrier in the rebound step.^[62] The oxidation-state changes, discussed above, which attend the rebound process correspond to an avoided crossing of the characteristic VB structures that possess these oxidation states. A typical VB diagram is shown in Figure 9, along a “reaction coordinate” that converts the ferryl re-

bound cluster (at the left hand extreme) to a ferric–alcohol complex (at the right hand extreme). A similar diagram will correspond to the conversion of the ferric intermediate, $\text{C}_1(\text{III})$, to the ferric–alcohol product. These valence-bond crossing patterns were recently verified computationally by creating the vertical states of the diagram and subsequently monitoring their crossover through the changes in charge and spin density on the alkyl group during the HS and LS rebound pathways for the substrate *trans*-1-isopropyl-2-phenylcyclopropane.^[63]

The ground state, on the left-hand side, corresponds to a ferryl, $\text{C}(\text{IV})$, cluster. The excited state involves an *ion-pair* that corresponds to the vertical state in which the electron from the alkyl radical has been shifted to the iron–hydroxo moiety, to an orbital that depends on the spin state and oxidation state of the iron–hydroxo species, as discussed above in Figure 7. The vertical excited state correlates directly to the ground state of the alcohol complex product, on the left-hand side, since they possess essentially the same electronic structure. On the other hand, the ground state on the left-hand side correlates to an excited state of the alcohol product complex, in which one electron is excited from the $\pi^*(d_{xz})$ orbital into the $\sigma^*(\text{C–O})$ orbital. Since the two VB states have the same symmetry properties, they can mix with each other and avoid the crossing leading to an adiabatic state, which is lower by an amount B than the crossing point, and which corresponds to the transition state for rebound.

The rebound barrier is given by the following equation:^[62]

$$\Delta E_{\text{reb}}^{\ddagger} = fG - B; f < 1 \quad (1)$$

Here, G is the vertical gap between the VB structures at the onset of the diagram, and f is the fraction of this excitation gap that enters under the crossing point of the VB

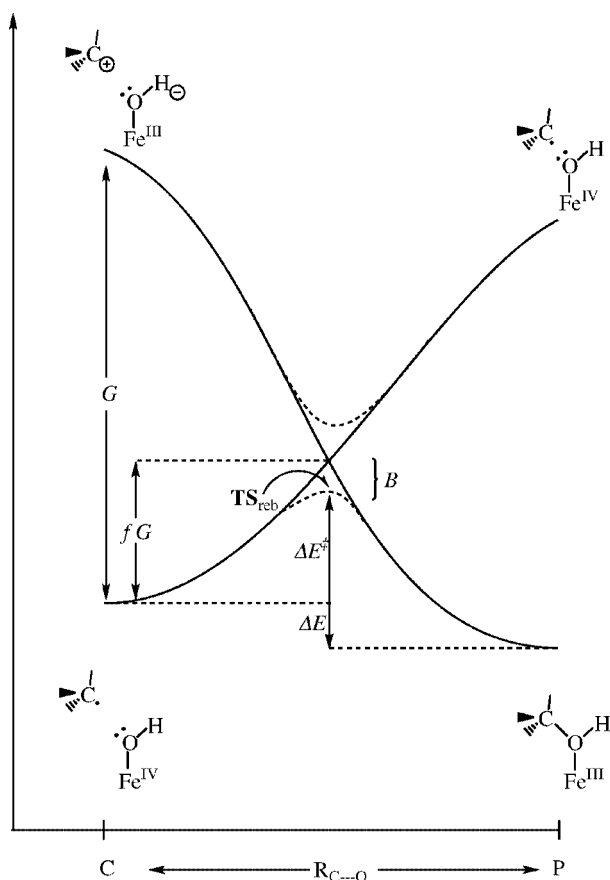


Figure 9. A valence-bond diagram (see ref.^[62]) showing the origin of the rebound barrier; G is the vertical energy gap between the ground state of the rebound cluster, exemplified by $C(IV)$ and the excited state where an electron was shifted to the iron d orbital; in the **LS** process the electron is shifted to the low-lying π^* orbital (on the FeO moiety), while in the **HS** rebound the electron is shifted to the high-lying $\sigma^*(d_z^2)$ orbital; the quantity fG corresponds to the height of the crossing point, B to the quantum mechanical resonance energy due to the mixing of the valence bond forms, and ΔE to the energy difference between the cluster and the alcohol complex product

state curves. Finally, B is the VB mixing energy at the crossing point.

The vertical gap, G , depends on the spin state and is given by the following expression:

$$G_{\text{HS}} = IP_{\text{Alk}} - EA_{\text{FeOH}} + E_{\text{el}} + \Delta E_{\pi^* \rightarrow \sigma^*} \quad (2a)$$

$$G_{\text{LS}} = IP_{\text{Alk}} - EA_{\text{FeOH}} + E_{\text{el}} \quad (2b)$$

where IP is the ionization potential, EA the electron affinity, and E_{el} the electrostatic energy in the ion pair. The **HS** gap is seen to involve the additional excitation energy term, $\Delta E_{\pi^* \rightarrow \sigma^*}$, to the $d_z^2(\sigma^*)$ orbital. Calculated at the LACVP(6-31G) level, this quantity is ca. 24 kcal·mol⁻¹. The second factor, f , depends, inter alia, on the thermodynamic driving force of the rebound step, ΔE , and becomes smaller the more exothermic the rebound is.^[62] Since the **LS** rebound is considerably more exothermic (Figure 2)

than the **HS** rebound (e.g. by 13 kcal·mol⁻¹ for allyl rebound), the f factor will depend on the spin state such that:

$$f_{\text{LS}} < f_{\text{HS}} \quad (3)$$

Therefore the height of the crossing point for the **LS** rebound will be considerably smaller than that for the **HS** rebound:

$$f_{\text{LS}}G_{\text{LS}} \ll f_{\text{HS}}G_{\text{HS}} \quad (4)$$

The calculated gas-phase electron affinity of the iron–hydroxo species is quite large, 63 kcal·mol⁻¹ at the LACVP(6-31G) level, and in a polarizing medium ($\epsilon = 5.7$) it goes up to about 100 kcal·mol⁻¹. The IP of radicals like allyl or cyclopropylcarbinyl is 180 kcal·mol⁻¹, and it goes down further in a polarizing medium [for allyl radical $IP(\epsilon = 5.7) = 131$ kcal·mol⁻¹]. Thus, after inclusion of the electrostatic interaction, E_{el} , between the cation and the anion, the gap factor for the **LS** process of typical radicals (allyl, cyclopropylcarbinyl, etc.) would be rather small — $G \approx 60$ kcal·mol⁻¹. Using a typical value of $f = 0.25$, the fG term will be rather small, approximately 15 kcal·mol⁻¹. Since VB mixing further lowers the state by an amount B , which itself is of the order of 15 kcal·mol⁻¹,^[62] the **LS** rebound barrier will have an exceedingly small value or be virtually eliminated, as indicated by the DFT calculations. By contrast, the barrier for the **HS** rebound will persist and be significant, due to the additional excitation to the $d_z^2(\sigma^*)$ orbital and the poorer exothermicity factors. Using the computed values of the **HS** excitation energy, $\Delta E_{\pi^* \rightarrow \sigma^*}$, and a typical value for f ($f = 0.25$)^[62] predicts that the **HS** barrier will be 6 kcal·mol⁻¹ higher than the **LS** process. This is not too far from the DFT-computed difference.

The role of the excitation term to the $d_z^2(\sigma^*)$ orbital is further illustrated by the dependence of the barrier on the identity of the proximal ligand (Table 1). Thus, for thiolate, which interacts strongly with the iron atom, the $d_z^2(\sigma^*)$ orbital is high and the rebound barrier is significant. By contrast, imidazole (ImH) and methyl sulfonate (MeSO_3^-) proximal ligands, which are much poorer σ -binders, have much lower $d_z^2(\sigma^*)$ orbitals,^[64] and consequently their rebound barriers decrease and virtually disappear, as seen in Table 1 (Entries 8 and 9).

A more striking effect is caused by changing the transition metal, i.e., when iron is replaced by ruthenium (Table 1). The 4d orbitals of ruthenium overlap much better with the 2p orbitals of the oxygen atom than the 3d orbitals of the iron atom.^[28,65] Consequently, the $\sigma^*(d_z^2)$ orbital of the ruthenium–hydroxo species is much higher than the corresponding orbital of the iron–hydroxo one. This is the reason why the rebound barrier for ruthenium is almost four times larger than the corresponding barrier for iron.

The dependence of the **HS** rebound barrier on the oxidation state of the iron atom in the iron–hydroxo species can be understood by consideration of the term B in Equa-

tion (1), by appeal to Figure 7. This term can be viewed as the C...O bonding energy in the transition state and along the rebound path. In the ferryl(IV) situation, the electron is shifted from the radical center directly to the $d_z^2(\sigma^*)$ orbital, and hence $B(\text{IV})$ is simply proportional to the overlap of these two orbitals, namely, $\langle\phi_{\text{C}}|d_z^2(\sigma^*)\rangle$. By contrast, in the ferric(III) situation, the electron cannot be shifted directly to $d_z^2(\sigma^*)$ due to spin frustration. Instead, while the spin-up electron in the ϕ_{C} orbital shifts into $d_z^2(\sigma^*)$, the spin-down electron in π^*_{xz} has to shift to a_{2u} to fill this orbital. Due to this higher order reorganization of the electronic structure, the factor $B(\text{III})$ is proportional to a product of orbital overlaps of the orbitals which participate in this electronic reshuffle, $\langle\phi_{\text{C}}|d_z^2(\sigma^*)\rangle\langle\pi^*_{xz}|a_{2u}\rangle$, and is hence smaller, namely:

$$B(\text{IV}) > B(\text{III}) \quad (5)$$

Since the two **HS** rebounds have approximately the same G and f factors, the stronger VB mixing for the ferryl situation will give rise to a smaller rebound barrier, as is indeed reflected by the data in Table 1.

Finally, further consideration of the term B shows that the rebound trajectory of the **LS** and **HS** processes must be quite different. In the **HS** rebound the electron shifts from the radical center to the $d_z^2(\sigma^*)$ orbital. Hence, to maximize the bonding term, B , the $^4\text{TS}_{\text{reb}}$ species must assume a structure with a large $\angle\text{FeOC}$ angle, as is indeed shown in Figure 5 ($\angle\text{FeOC} \approx 160^\circ$). By contrast, since the **LS** rebound [in the C(IV) electromer] involves a shift of the electron from the alkyl radical to the π^*_{xz} orbital, maximization of the O...C bonding along the rebound pathway requires an $\angle\text{FeOC}$ angle of $\geq 90^\circ$. When one of these angular requirements cannot be met due to steric constraints, the corresponding barrier will increase. Such a case was recently encountered^[63] in the rebound of aryl radicals, which resulted in rebound barriers in both **HS** and **LS** manifolds, since the required $\angle\text{FeOC}$ angle of $\geq 90^\circ$ for the **LS** path was barred by steric effects. These cases will not be discussed any further in the present Microreview.

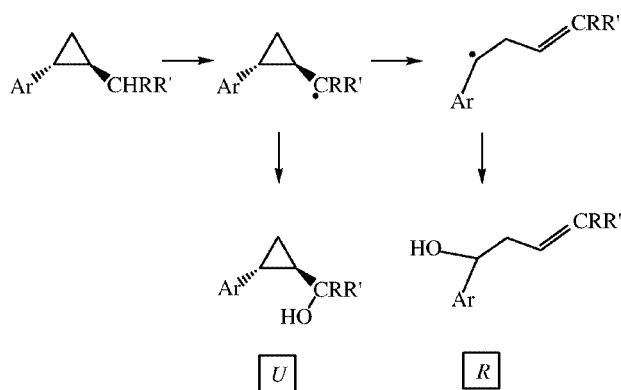
Rearrangement Patterns of Radical Clocks

Clearly, the VB model in Figure 9 provides a consistent framework for analyzing and predicting trends in the rebound process. Let us now consider a series of probe substrates, which can form radicals that can undergo skeletal rearrangement, so that the unrearranged (U) and rearranged (R) forms of the radical can rebound and give rise to corresponding alcohol products, U and R , like the clock probes used by Newcomb et al.^[15] The negative results of the slow clocks cannot be analyzed, but they enable us at least to bracket the barrier of the **HS** rebound to be smaller than the barrier for a slow probe like cyclopropyl carbinyl radical, which has a rearrangement barrier of approximately $6.9 \text{ kcal}\cdot\text{mol}^{-1}$.^[57] There are, however, $[U/R]$ data that can be analyzed, and the question is: What can we

predict for the measurable quantity $[U/R]$, in a clock experiment?

For simplicity, we must consider a case where the only competing processes are the radical rearrangement and the **HS** and **LS** rebounds. Assuming that the **LS** rebound is effectively concerted, giving rise to only U products, and that the radicals on the **HS** manifold can give rise to both U and R , we can then make some predictions about the behavior of the quantity, $[U/R]_{\text{HS}}$, that arises from the **HS** rebound. A clear prediction can be made when the series meets the following conditions: (i) the rearrangement rate of the radicals is constant or quasi constant, (ii) the thermodynamics of the **HS** rebound does not vary in an adverse manner to the gap, and (iii) the rearrangement of the radical is irreversible, such that all rearranged radicals end up as rearranged alcohols.

The VB model (Figure 9) and the equation for the barrier [Equations (1) and (2)] tell us that when the above conditions hold true, the rebound barrier, $\Delta E_{\text{reb}}^\ddagger$, will depend on a single factor, the IP_{Alk} of the radical (within the protein pocket). The smaller the IP_{Alk} quantity, the lower the rebound barrier will be, and the shorter will be the radical lifetime on the **HS** manifold. Thus, for the above conditions, we expect that the $[U/R]_{\text{HS}}$ quantity, as well as the total $[U/R]$, will increase as the IP_{Alk} decreases, i.e., as the radical becomes a better electron donor. Such a series was investigated by Newcomb et al.^[15,17] who used clocks that are structurally related and have virtually identical rearrangement rate constants of ca. 10^{11} s^{-1} . These clocks are arranged in Scheme 5, in order of donor ability of the corresponding radical, and along with the measured $[U/R]$ quantities. It can be seen that, in this series, which meets



probe	Ar	R,R'	IP_{Alk}	$[U/R]$
2	<i>p</i> CF ₃	H, H	highest	4
3	<i>p</i> H	H, H		4.3
4	<i>p</i> CF ₃	H, CH ₃		12
5	<i>p</i> H	H, CH ₃		25
6	<i>p</i> H	CH ₃ , CH ₃	lowest	> 100

Scheme 5. A rebound/rearrangement scheme for probe substrates (ref.^[15]) and the variation of their $[U/R]$ quantities with the ionization potentials of the corresponding alkyl radicals

approximately the requirements stated above, the $[U/R]$ quantity increases rapidly, with decrease of IP_{Alk} , from 4 to more than 100, as predicted by the above simple consideration. Our most recent calculations of the best donor substrate, **6**, in this series shows that, indeed, the **HS** rebound barrier vanishes, and as such both the **LS** and **HS** processes become effectively concerted.^[63]

Interestingly, Newcomb, Lippard et al.^[20,57] found that for MMO hydroxylation the probe substrate **3** gave no rearrangement at all, as opposed to the approximately 25% of rearranged alcohol observed during P450 hydroxylation of the same probe. This can be understood by recognizing that the electron affinity of the iron–hydroxo form of the enzyme MMO is significantly larger than that of the iron–hydroxo species of P450. As such, the energy gap factor, G [Equation (2)], for MMO rebound processes will generally be smaller than the same gap in P450 rebounds, leading to less rearranged products.

An interesting trend that can be predicted from the VB model refers to the effect of the strength of Fe–S binding on the **HS** rebound barrier. Weak binding will lower the energy of the $d_z^2(\sigma^*)$ orbital, and will therefore decrease the **HS** rebound barrier. Since rebound and rearrangement compete with one another, enhancement of the rebound rate will, in turn, decrease the amount of observed rearranged product. The polarity and acidity of the protein pocket affect the strength of the Fe–S bonding,^[46,64,66,67] and one might therefore expect to find that the $[U/R]$ quantity is different for different P450 isozymes. This conclusion means that $[U/R]$ is not a pure property of the clock probe. Furthermore, studies by Newcomb et al.^[38,68] and by Ortiz de Montellano and Groves et al.^[21] show dependencies of the $[U/R]$ quantity on the P450 isozyme. While we cannot rationalize the precise trends we can at least point out that the VB model predicts such behavior as the result of the variation of the Fe–S bonding with the identity of the isozyme. Presumably, this kind of information on the Fe–S bonding can ultimately be obtained by crystallography and spectroscopy.^[66,69] Such a dependence of the $[U/R]$ quantity on the identity of the isozyme is a clear demonstration that $[U/R]$ does not measure intrinsic lifetimes of the radicals. Therefore one does not expect to find a correlation between this quantity and the rate of free-radical rearrangement, as indeed demonstrated in the study of Newcomb et al.^[15]

What Does the $[U/R]$ Quantity Actually Measure?

The above discussion considers the $[U/R]_{\text{HS}}$ quantity that arises from the **HS** rebounds. However, the rebound also involves an **LS** component, and hence the total $[U/R]$ quantity is a two-state information that must also be associated with the relative **LS/HS** yields, and not only with lifetimes as such. The question we wish to address here is: What mechanistic information is provided by the measured $[U/R]$ quantity? One apparent aspect of the “rebound controversy” is that while the slow clocks do not lead to rearranged products, with the notable exceptions of norcaradiene and bicyclo[2.1.0]pentane,^[20,21] the fast clocks undergo rearrangement, but lead to apparent lifetimes that are too

short, sometimes as short as 70 fs.^[15] Using the two-state approach enables us to understand this aspect, by appeal to Figure 2, and assuming that the **LS** pathway is effectively concerted (or leading to a negligible amount of rearranged products).

At the limit of independent **LS** and **HS** pathways with initial fractions n and $(1 - n)$, respectively, the actual rate of rebound on the **HS** manifold is given by:^[23,26]

$$k_{\text{reb}}^{(\text{HS})} = k_{\text{r}} \{ [U/R]_{\text{tot}} - F_{\text{LS/HS}} \} / \{ 1 + F_{\text{LS/HS}} \};$$

$$F_{\text{LS/HS}} = [n/(1 - n)] k_{\text{LS}}/k_{\text{HS}} \quad (6)$$

Here, k_{LS} and k_{HS} correspond to the rate constants for C–H bond activation for the **LS** and **HS** states, respectively, while $[U/R]_{\text{tot}}$ is the total ratio of unrearranged to rearranged products obtained from the two states:

$$[U/R]_{\text{tot}} = [(U_{\text{HS}} + U_{\text{LS}})/R_{\text{HS}}] \quad (7)$$

The apparent rebound rate, which is quantified simply from the measured $[U/R]_{\text{tot}}$ quantity, is given on the other hand by:

$$k_{\text{reb}}^{(\text{app})} = k_{\text{r}} [U/R]_{\text{tot}} \quad (8)$$

The lifetimes are inversely related to the rate constant of the rebound, and hence the ratio of the actual lifetime of the radical, on the **HS** manifold, to the apparent lifetime will be given by:

$$\tau^{(\text{HS})}/\tau^{(\text{app})} = \{ [U/R]_{\text{tot}} (1 + F_{\text{LS/HS}}) \} / \{ [U/R]_{\text{tot}} - F_{\text{LS/HS}} \} > 1 \quad (9)$$

Clearly, the apparent lifetime is shorter than the actual one. The difference may be small if the relative yield quantity, $F_{\text{LS/HS}}$, is close to unity. In such a case, the apparent lifetime is a reasonable approximation to the actual lifetime of the radical in the **HS** manifold. If, however, k_{LS} is significantly larger than k_{HS} and/or $n \gg (1 - n)$, the result is that $F_{\text{LS/HS}} \gg 1$. In such a situation, the apparent lifetime will be much shorter than the actual one, leading to absurdly short lifetimes. Our recent computations of allylic hydroxylation show that under conditions that mimic the polarity and hydrogen bonding in the protein pocket, $k_{\text{LS}}/k_{\text{HS}}$ is approximately 10.^[27,49] With such values of $F_{\text{LS/HS}} \approx 10$, the apparent lifetime [Equation (8)] will be absurdly short.

In the general situation, $F_{\text{LS/HS}}$ is predicted to increase^[23] with the improved donor ability of the alkane, and hence to vary as the measured $[U/R]_{\text{tot}}$ quantity itself. Thus, in a series such as the Newcomb clocks in Scheme 5, the value of $F_{\text{LS/HS}}$ will vary; its meaningful variation is limited by the requirement to produce only positive lifetimes. For example, with the probe **3** (Scheme 5), for which $[U/R]_{\text{tot}} \approx 4$, $F_{\text{LS/HS}}$ should be < 4 (to yield a positive lifetime), while with the best donor probe, **6**, where $[U/R]_{\text{tot}} > 100$, $F_{\text{LS/HS}}$

is much larger since in this case both **HS** and **LS** processes rebound in a barrierless fashion,^[63] such that, in fact, $[U/R]_{\text{tot}} \rightarrow \infty$. In any event, the actual lifetime will be longer than the apparent one by a factor N :

$$\tau^{(\text{HS})} = N \cdot \tau^{(\text{app})}; N > 1 \quad (10)$$

For example, taking N to be equal to 10, the values of $F_{\text{LS/HS}}$ that will yield positive lifetimes must vary from < 3 to 9 in the Newcomb series in Scheme 5, while for $N = 5$, $F_{\text{LS/HS}}$ varies between < 2 and 4. This range of $F_{\text{LS/HS}}$ variation is reasonable, as can be judged from the DFT calculations that indicate preponderance of the **LS** process. Thus, we may bracket the value of N in Equation (10) between 5 and 10. With such N values in Equation (10), the radicals in the Newcomb series will possess real lifetimes of the order of picoseconds, which are reasonable lifetimes. Clearly, since the $[U/R]_{\text{tot}}$ quantity is a two-state information content, it does not measure the actual lifetime of the intermediate *but depends strongly on the relative yields of HS and LS reaction fluxes for a given total yield of products*.

There exist alternative scenarios, which can potentially reconcile the “rebound controversy”. The common element to all the alternative models is that the apparent lifetime reflects the interplay of effects not present in a single state rearrangement of the “free radical”. Let us mention three such alternative scenarios.

One possibility that has been proposed^[3,10,60] is that, inside the protein, radical clocks rearrange much slower than the corresponding “free radicals”, due to stereoelectronic constraints. This alternative has never been tested seriously, and merits evaluation. It will not, however, rule out the concomitant validity of the two-state picture.

The second scenario is the two-oxidant hypothesis^[15] (Scheme 2), in which the second oxidant inserts hydroxonium ion and leads to rearrangements by anchimeric assistance typical to carbocations without having free carbocation intermediates. The problem with this otherwise perfectly legitimate hypothesis is the unknown nature of the second electrophilic oxidant. Ferric hydroperoxide, Cpd 0 (Figure 1), was tested and found to possess huge barriers for epoxidation^[39,70] and sulfoxidation^[40] compared with the same processes with Cpd I. This at least rules out the reactivity of Cpd 0 in the presence of Cpd I. Moreover, the sulfoxidation study^[40] shows that the barrier would still be high even if the reaction of Cpd 0 were to be catalyzed by a potent proton source like H_3O^+ coordinated by a single water molecule. Thus, Cpd 0 appears to be a poor electrophile, which is expected to react only in the absence of Cpd I. Recent evidence shows that in mutants of P450, where the primary machinery of proton delivery that converts Cpd 0 to Cpd I is disrupted, the enzyme can still perform epoxidation but very sluggishly, and *it loses completely its hydroxylation capability*.^[42] Thus, even if Cpd 0 functions as an oxidant, it is still doubtful, at least at the present state of experimental and theoretical understanding, that Cpd 0 can play a role in the hydroxylation mechanism.

The third alternative emerges from a recent study of a semiclassical molecular dynamics simulation of ethane hydroxylation by the enzyme MMO.^[32] Applying this scenario to P450 requires a single intermediate species, which is the $^4\text{C}_1$ intermediate, $\text{FeOH}\cdots\text{C}(\text{Alk})$, generated by a hydrogen-abstraction step. Since the hydrogen-abstraction transition state lies above the rebound transition state, part of the total reaction flux can bypass the intermediate and proceed in an effectively concerted process. In this process, the fast energy transfer of the excess energy to the OH rotational mode that is active in the rebound can carry the hydrogen-abstraction transition state directly to the final hydroxylation product, without residing in the well of the $\text{OH}\cdots\text{C}(\text{Alk})$ intermediate. This concerted process results in alcohol products that conserve the stereochemical identity of the alkane. The other part of the reaction flux will pass through the well of the $\text{OH}\cdots\text{C}(\text{Alk})$ intermediate, and be partitioned between rebound and rearrangement modes giving rise to a mixture of unrearranged and rearranged products. Thus, here too the $[U/R]_{\text{tot}}$ quantity reflects the interplay of two processes, one effectively concerted and the other stepwise, precisely as described above for the two-state scenario. Moreover, using the VB model (Figure 9) coupled to the dynamic scenario for analyzing the trends in the barrier of the stepwise component can, in principle, rationalize the behavior of the Newcomb probe series (Scheme 5). However, to be considered equally valid for the P450 enzyme, the dynamic scenario must fulfil the following two requirements. Firstly, the dynamics^[32] have to be done within the protein environment, where fast dissipation of the excess energy to the protein modes may minimize the concerted component. Secondly, a proper dynamic study should prove or disprove the two-state scenario by including this aspect of the problem. Should such a study be carried out, and *should it indeed rule out the participation of two states*, this would then favor an original Groves mechanism,^[59] within the formulation of a “bound radical”.^[32,54,55] Still, however, any mechanistic model of alkane hydroxylation must meet the challenge described in the following section.

The Product Isotope Effect and Its Mechanistic Significance in TSR

A product isotope effect (PIE) in the context of alkane hydroxylation means that when the hydrogen atom that is transferred from the alkane to the iron–oxo moiety is replaced by a deuterium atom, the product ratio $[U/R]$ will exhibit an isotope effect. *The observation of such an isotope effect means necessarily that the products U and R cannot be generated from a single intermediate or pathway and must be mediated by two pathways or from two sources*. The two-state scenario predicts that there should, in principle, be a product isotope effect (PIE) on the $[U/R]$ quantity, since *U* and *R* are produced from two pathways.^[45]

To derive a simplified expression for the PIE, we assume that the rearranged alcohol is generated only on the **HS** process, and this leads to the following equation for the isotope effect on the $[U/R]$ quantity:

$$\frac{[U/R]_{\text{H}}}{[U/R]_{\text{D}}} = \text{PIE}[U/R] = \frac{[(k_{\text{HS}}^{\text{H}}/k_{\text{LS}}^{\text{H}})/(k_{\text{HS}}^{\text{D}}/k_{\text{LS}}^{\text{D}})]\{(k_{\text{r}}^{\text{H}}/k_{\text{r}}^{\text{D}})[(k_{\text{reb}}^{\text{H}}/k_{\text{reb}}^{\text{D}})/(1 + k_{\text{r}}^{\text{D}}/k_{\text{reb}}^{\text{D}})]\}}{(1/\text{IE}_{\text{LS}}/\text{IE}_{\text{HS}})\{(1/\text{IE}_{\text{r}})[(k_{\text{r}}^{\text{H}}/k_{\text{reb}}^{\text{D}} + \text{IE}_{\text{reb}})/(1 + k_{\text{r}}^{\text{D}}/k_{\text{reb}}^{\text{D}})]\}} \quad (11)$$

Thus, the $\text{PIE}[U/R]$ should depend on the ratio of intrinsic isotope effects (IEs) of the **HS** and **LS** hydrogen-abstraction steps (i.e. $\text{IE}_{\text{LS}}/\text{IE}_{\text{HS}}$), the isotope effect of rearrangement process (i.e. IE_{r}), and that of the rebound process (i.e. IE_{reb}). In the events that the rearrangement and rebound processes do not exhibit isotope effect, the expression becomes very simple, and depends only on the intrinsic IE ratio of the **LS** and **HS** hydrogen-abstraction steps, namely:

$$\text{PIE}[U/R]_{\text{TSR}} \approx \text{IE}_{\text{LS}}/\text{IE}_{\text{HS}} \quad (12)$$

As such, for those systems where rearrangement and rebound processes are not subject to an isotope effect, the $\text{PIE}[U/R]$ quantity can be predicted by straightforward DFT calculations of IE_{LS} and IE_{HS} . Using this equation, it is easily apparent that the two-state scenario would predict a product isotope effect, namely $\text{PIE}[U/R] \neq 1$ unless the **HS** and **LS** transition states (TSs) happen to have accidentally identical structures, which they usually do not. Furthermore, the two-state mechanism predicts a substrate-dependent $\text{PIE}[U/R]$, and this dependency can be understood by recalling,^[5] that the maximal IE value is expected when the hydrogen-abstraction TS is “central” (i.e., having identical $\text{C}\cdots\text{H}$ and $\text{H}\cdots\text{O}$ bond orders/lengths), while smaller values are expected for TSs that are either “early” or “late”. Thus, *the direction of the intrinsic $\text{PIE}[U/R]$ (< 1 or > 1) quantity will generally reflect the relative positions of the hydrogen-abstraction transition states along the reaction coordinate, for the **HS** and **LS** processes.*

The ratios $\text{IE}_{\text{LS}}/\text{IE}_{\text{HS}}$ were computed for the hydroxylation of methane,^[45] propene,^[27] ethane,^[29,30] camphor,^[31] and *trans*-1-methyl-2-phenylcyclopropane.^[61] In the cases of methane, ethane and propene, the ratios are < 1 , of the order of 0.7–0.8, while for camphor,^[31] these ratios are either > 1 or close to 1, depending on the pattern of isotopic substitution, and on whether the IEs are inter- or intramolecular. Finally, for *trans*-[D₂]-1-methyl-2-phenylcyclopropane, the computed^[61] intramolecular $\text{PIE}[U/R]$ is 1.083–1.223, where the larger values include the effect of tunneling. Similarly, calculation of this quantity^[61] for the intermolecular isotope effect (i.e., *trans*-1-methyl-2-phenylcyclopropane vs. *trans*-[D₃]-1-methyl-2-phenylcyclopropane) led to $\text{PIE}[U/R]$ values of 0.943–1.123 where, again, the larger values involve strong tunneling correction. Other cases we studied,^[63] show that the ratio of $\text{IE}_{\text{LS}}/\text{IE}_{\text{HS}}$ can deviate from unity by as much as 40%, depending on the substrate.

Earlier experimental data by Newcomb and Ingold^[37] for the two enantiomers of *trans*-1-methyl-2-phenylcyclopropane revealed ambiguous results, with values both smaller and larger than unity, $\text{PIE}[U/R] \approx 0.6$ –1.09, for the intermolecular isotope effect (i.e., *trans*-1-methyl-2-phenylcyclopropane vs. *trans*-[D₃]-1-methyl-2-phenylcyclopropane). By

contrast, more recent data of Newcomb et al.^[38] led to values larger than unity (e.g., the average $\text{PIE}[U/R] \approx 1.143$) for the intramolecular isotope effect (using *trans*-[D₂]-1-methyl-2-phenylcyclopropane); the corresponding computed values using the TSR scenario^[61] are 1.083–1.223. Despite this good agreement between theory^[61] and the latter experimental results,^[38] some qualification is in order. The experimental results are sensitive to very small changes in the percentages of the products, and gas chromatographic analysis of product distribution is subject to errors of 1–2%.^[5] As such, without a proper error analysis, the recent experimental study^[38] only shows that the $[U/R]$ product ratio is likely to exhibit an isotope effect. Such an isotope effect means that the products *U* and *R* are generated by two pathways or from two sources. In this sense, the experimental results suggest the operation of TSR in alkane hydroxylation. However, should the experimental values^[38] prove to be accurate, then the match between experiment and TSR theory will be a proof of principle for the operation of TSR in alkane hydroxylation.

Are There Carbocation Intermediates in P450 Hydroxylation?



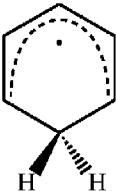
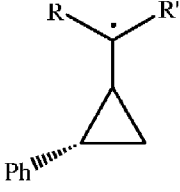
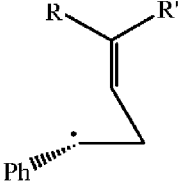
Newcomb et al. have devised probes that can distinguish between cationic and radical rearrangements. One of these probes, **1** in Scheme 2, opens at the C–C bond that has an alkoxy substituent, which is the rearrangement mode expected for a carbocation intermediate. Similarly, Ortiz de Montellano, Groves et al.^[21] and Newcomb et al.^[20] have observed rearrangement products of norcarane that can be associated with a carbocationic rearrangement. However, Newcomb et al.^[15] do not actually invoke free carbocations, but rather describe this typical rearrangement mode as being due to the presence of a protonated alcohol (nascent from OH^+ insertion, Scheme 2). By contrast, Ortiz de Montellano, Groves et al.^[21] ascribe the small yield of these products to the presence of free carbocations generated by electron transfer (ET):



Right from the outset, it should be apparent that the ET process bears a resemblance to the rebound step, in the sense that in both cases the same two VB structures intersect (Figure 9). However, while during the rebound process this intersection occurs along a bond-making trajectory with a large VB mixing term *B*, and favorable exothermicity, in the ET process this will have to occur in an outer-sphere manner, with $B \rightarrow 0$, along a trajectory that avoids bond making and is thermodynamically less favorable. This typical competition between related bond-making and ET processes is well known,^[62] and the bond-making process prevails unless bonding is blocked.

To assess the feasibility of ET, we calculated the energy change, ΔE_{ET} , of the reaction for a variety of alkyl radicals, using the ionization potential data in Table 2. The electron

Table 2. Ionization potentials (in eV units) of a few radicals^[a]

Entry	Radical	IP^v	IP^{ad}
1		8.05 (8.06)	~8.05
2		7.40	7.38
3		7.19	7.14
	 		
	(closed) (open)		
4, R = R' = H			
4a	(closed)	7.97	
4b	(opened)	7.07	
5, R = H; R' = CH ₃			
5a	(closed)	7.65	
5b	(opened)	7.03	
6, R = R' = CH ₃			
6a	(closed)	7.40	
6b	(opened)	7.00	

^[a] Calculated with the Green's function technique as described in refs.^[74,75]

affinity of the iron–hydroxo species is 63 kcal·mol^{−1} in the gas phase, and 100 kcal·mol^{−1} in a polarizing medium with $\epsilon = 5.7$. As we showed recently,^[64] the thiolate ligand hampers the electron-acceptor properties of iron–porphyrin species, relative to non-thiolated alternatives, by as much as 30 kcal·mol^{−1} in a polarizing medium (and much more, 50–100 kcal·mol^{−1}, in the gas phase). Thus, with MMO, where the electron affinity of the diiron–hydroxo species is expected to be larger than the P450-derived iron–hydroxo one, the incursion of a carbocation species would be very much more feasible than in P450. Therefore, evidence of the presence of carbocations in MMO hydroxylations cannot constitute a proof for their existence also in the P450 reaction, unless the radical is a very good electron donor. For a radical like allyl, with calculated $IP_{\text{allyl}} = 186$ kcal·mol^{−1} (131 kcal·mol^{−1} in $\epsilon = 5.7$) the electron-transfer reaction in Equation (13) is endothermic by 31 kcal·mol^{−1}. Even after inclusion of electrostatic interactions of ca. 14 kcal·mol^{−1} (for an ion-pair at 3 Å in an effective dielectric constant of a protein), the ET reaction is still endothermic. This should be the case for all the radicals in Table 2. How-

ever, for probes with $IP_{\text{Alk.}} < 160$ kcal·mol^{−1} (< 106 kcal·mol^{−1} in $\epsilon = 5.7$), one might anticipate an exothermic ET reaction with diffusive cationic species.

A bound carbocation that is coordinated to an iron–hydroxo anion is more likely to exist than a diffusive one. For example, in our recent study of benzene hydroxylation, we located an oxopentadienyl carbocation intermediate coordinated to the heme anion.^[71] This carbocationic intermediate becomes more stable (by 4.9 kcal·mol^{−1}) than the corresponding radical in a polarizing medium ($\epsilon = 5.7$). However, as shown in Figure 10a, the charge on the phenyl group (Q_{Ph}) is significantly less than unity. The species is therefore an intimate ion-pair with a significant degree of electronic conjugation between the radical and the iron–hydroxo moieties. To test the situation with a typical Newcomb probe system, we calculated^[61] the putative cationic intermediate that can derive from *trans*-1-methyl-2-phenylcyclopropane, shown in Figure 10b. This is done by shifting the electron from the radical center on the organic moiety to the heme singly occupied orbital (π^* or a_{2u} orbital), and then letting the resulting species optimize its

electronic structure. From the charges on the alkyl moiety (0.18–0.27), it is apparent that this species is not an ion-pair; the charge on the organic moiety is simply too small, as might be expected from its relatively high *IP* (Entry 4a in Table 2). A natural orbital analysis indicates that the species behaves as a mixed-valent state, where the electron resides partly on the radical and partly on the porphyrin in the a_{2u} orbital. This feature is depicted in Scheme 6, alongside the drawing of the natural orbitals that contain the population of 1.5 and 0.5 e^- . These orbitals are the bonding and antibonding combinations of the radical orbital, ϕ_C , and the a_{2u} orbital (the mixing is mediated by the π^* orbitals of the FeO moiety). As such, this species is mostly the $\text{Fe}^{\text{III}}\text{Por}^+(\text{R}^-)$ species with a minor contribution from an intimate ion-pair form, $\text{Fe}^{\text{III}}\text{Por}(\text{R}^+)$. Even the best electron-donor radical in the Newcomb series (Table 2, Entry 6a) has an *IP* value close to benzene-derived pentadienyl radical (Entry 3). As such, this radical, too, generates a mixed species with a charge of +0.6 on the alkyl moiety.^[63] It is doubtful that these species, even in the cases where they possess a large carbocationic character, will behave like free carbocations.

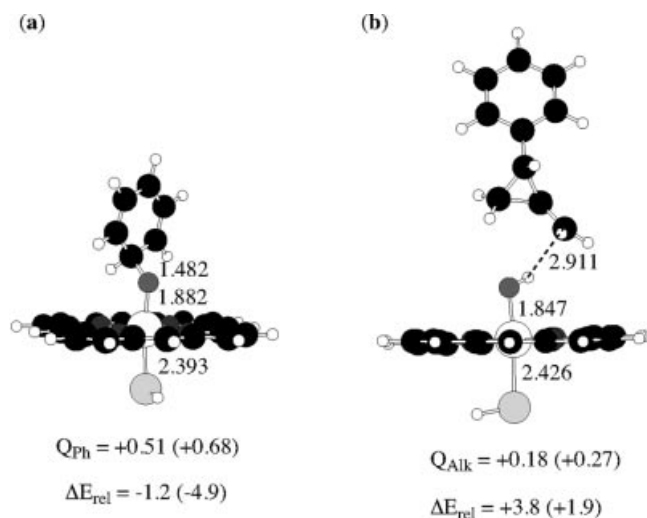
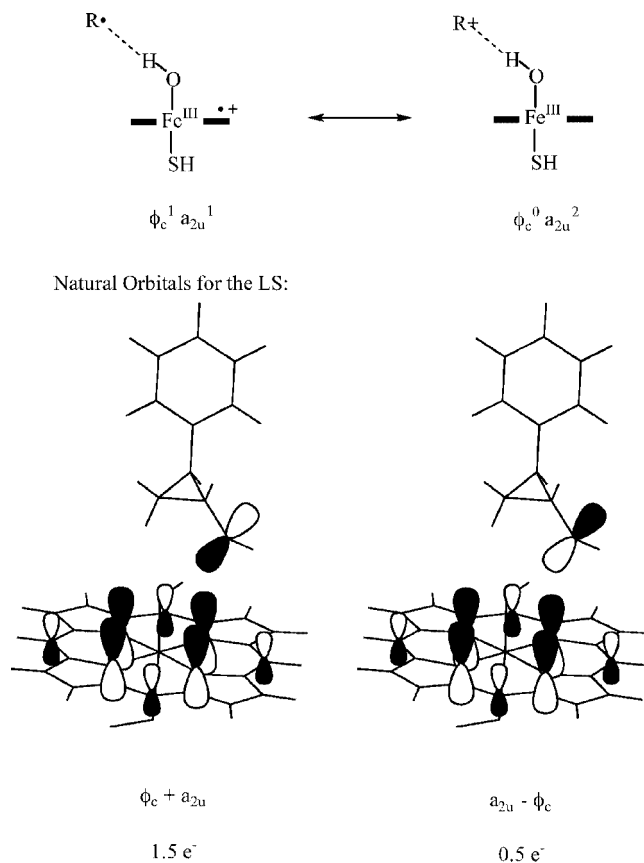
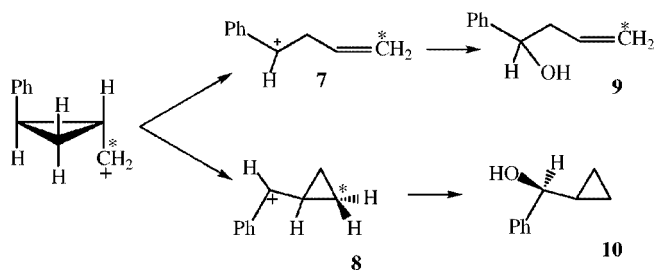


Figure 10. The geometric structures of (a) the ion-pair intermediate in benzene hydroxylation and (b) an analogous species in *trans*-1-methyl-2-phenylcyclopropane hydroxylation; below each structure we indicate the group charge of the organic moiety (*Q*) and the relative energy (ΔE_{rel}) to the radical intermediate (C_1) in vacuo (out of parentheses) and in a dielectric constant, $\epsilon = 5.7$ (in parentheses)

Our calculations of the rearrangement patterns of the free cation derived from *trans*-1-methyl-2-phenylcyclopropane reveals that the free cation would rearrange in a completely different manner than the corresponding radical, as summarized in Scheme 7. Alongside the “normal” rearrangement process to give **7**, the carbocation rearranges also to species **8**, in which the carbocation center is stabilized by both phenyl and cyclopropyl groups. The presence of **8** would have led to the hydroxylation product **10**, which, to the best of our knowledge, has never been reported.^[15] We may therefore conclude that free carbocations are not present in the chemistry of these particular probes.



Scheme 6. The resonance structures that describe the “intimate ion-pair” species; the drawing below corresponds to the natural orbitals, which are mixtures of the radical orbital, ϕ_C , and the a_{2u} orbital, for the “intimate ion-pair” species derived from *trans*-1-methyl-2-phenylcyclopropane depicted in Figure 10b



Scheme 7. The rearrangement patterns of “free” *trans*-2-phenylcyclopropylcarbonyl cation and the expected hydroxylation products

We cannot, however, rule out the presence of cations in other probes. Such cations can escape the intimate ion-pairing and be stabilized by the protein environment, subsequently undergoing typical rearrangements. How much of the carbocationic products does one expect? A direct ET to produce diffusive carbocations will always be less efficient than rebound or radical rearrangement (recall that the radical clocks rearrange very fast, e.g., $k_r \approx 10^{11} \text{ s}^{-1}$). This, in turn, would require that the amount of carbocation-derived products be smaller than the amount of radical-derived rearrangement. While some P450 hydroxylation data^[16,21] indeed show that the amount of cation-derived rearranged

product is marginally smaller than the amount of radical-derived products, other data^[18,20] show the opposite trend. Alternatively, a carbocation intermediate of the intimate ion-pair type can arise directly from the C–H bond-activation phase by a hydride-abstraction process that competes with the radical-type hydrogen-abstraction process. This mechanism has not been observed yet and needs to be proven. Clearly the appearance of carbocation-derived products remains enigmatic and there is place for future experimental and theoretical studies of this issue.

Conclusion

The rebound controversy touches the limits of experimental capabilities to pinpoint complex reaction mechanisms. In such cases, theory can complement experiment by suggesting new alternatives. The two-state reactivity (TSR) scenario, which is supported by theory, provides such a paradigm. In TSR, radicals are produced on two different spin-state surfaces, and thereafter they react differently; on the low-spin surface rebound is barrierless, and hence the lifetime of the radicals is far too short to produce any rearranged products, while on the high-spin surface there is a substantial barrier for rebound, and hence the lifetime of the radical is sufficiently long so that rearrangement may compete with product formation by rebound. This paradigm provides a satisfactory rationale for the controversial findings in the field, and makes some verifiable predictions. Is this success merely accidental? This will have to be answered by future articulations of the concept.

One of the predictions of TSR is that the ratio of unrearranged to rearranged products, $[U/R]$, is subject to an isotope effect that is substrate-dependent. Further complications in the TSR picture are caused by the presence of different electromeric states of the iron–hydroxo intermediates (Figure 2), and possibly of an intimate ion-pair carbocation, which has a mixed valent character, $\text{PorFeOH}^-\cdots\text{Alk}^+ \rightleftharpoons \text{PorFeOH}\cdots\text{Alk}'$. Finally, for sterically demanding rebound processes, as in the case of benzyl radicals for example, one may expect TSR with rebound barriers on both HS and LS manifolds. These aspects, as well as the spin crossover between the two spin states, still await a future treatment.

Theoretical Section

General Remarks: DFT calculations with the hybrid functional B3LYP were routinely used and are described in great detail in our work.^[23,25,27,39,67] The calculations were carried out with JAGUAR 4.1^[72] and GAUSSIAN 98 packages.^[73] The standard basis involves a double zeta basis set which is called LACVP(6-31G), involving, on the iron atom, a Friesner basis set matched to an effective core potential, and a Pople 6-31G basis set on all other atoms. For some specified species, we also used more extended basis sets: one with polarization and diffuse functions on all

heavy atoms, LACVP+*(6-31+G*), a fully polarized basis, LACVP**/6-31G**, and two triple zeta basis sets without and with polarization functions, LACV3P(6-311G) and LACV3P*(6-311G*). All species were characterized by geometry optimization and subsequent frequency calculations. Calculations of the species with a polarizing electric field were done with the solvent model in JAGUAR 4.1 (based on the Poisson–Boltzmann model) using a dielectric constant of $\epsilon = 5.7$ and a probe radius, for the solvent, of 2.72 Å. Vertical ionization potentials were calculated using the outer valence Green's function (OVGF) technique, written by one of us (D. D.) and implemented in AMPAC.^[74,75]

Acknowledgments

The research was supported in parts by grants (to S. S.) from the Israeli Science Foundation (ISF) and the German–Israeli Foundation (GIF).

- [1] *Cytochrome P450: Structure, Mechanisms and Biochemistry* (Ed.: P. R. Ortiz de Montellano), 2nd ed., Plenum Press, New York, **1995**.
- [2] J. T. Groves, G. A. McClusky, *J. Am. Chem. Soc.* **1976**, *98*, 859–861.
- [3] P. R. Ortiz de Montellano, J. J. De Voss, *Natl. Prod. Rep.* **2002**, *19*, 1–18.
- [4] J. T. Groves, G. A. McClusky, R. E. White, M. J. Coon, *Biochem. Biophys. Res. Commun.* **1978**, *81*, 154–160.
- [5] A. Sorokin, A. Robert, B. Meunier, *J. Am. Chem. Soc.* **1993**, *115*, 7293–7299.
- [6] M. H. Gelb, D. C. Heimbrook, P. Mäklönen, S. G. Sligar, *Biochemistry* **1982**, *21*, 370–377.
- [7] M. Sono, M. P. Roach, E. D. Coulter, J. H. Dawson, *Chem. Rev.* **1996**, *96*, 2841–2888.
- [8] W.-D. Woggon, *Top. Curr. Chem.* **1996**, *184*, 39–95.
- [9] J. T. Groves, Y.-Z. Han, in *Cytochrome P450: Structure, Mechanism and Biochemistry* (Ed.: P. R. Ortiz de Montellano) 2nd ed., Plenum Press, New York, **1995**, pp. 3–48.
- [10] B. Meunier, J. Bernadou, *Top. Catal.* **2002**, *21*, 47–55.
- [11] H. Fretz, W.-D. Woggon, R. Voges, *Helv. Chim. Acta* **1989**, *72*, 391–400.
- [12] P. R. Ortiz de Montellano, R. A. Stearns, *J. Am. Chem. Soc.* **1987**, *109*, 3415–3420.
- [13] C. Audergon, K. R. Iyer, J. P. Jones, J. F. Darbyshire, W. F. Trager, *J. Am. Chem. Soc.* **1999**, *121*, 41–47.
- [14] H. Lee, P. R. Ortiz de Montellano, A. E. McDermott, *Biochemistry* **1999**, *38*, 10808–10813.
- [15] M. Newcomb, P. H. Toy, *Acc. Chem. Res.* **2000**, *33*, 449–455.
- [16] M. Newcomb, R. Shen, S.-Y. Choi, P. H. Toy, P. F. Hollenberg, A. D. N. Vaz, M. J. Coon, *J. Am. Chem. Soc.* **2000**, *122*, 2677–2686.
- [17] P. H. Toy, M. Newcomb, P. F. Hollenberg, *J. Am. Chem. Soc.* **1998**, *120*, 7719–7729.
- [18] M. Newcomb, M.-H. Le Tadic-Biadatti, D. L. Chestney, E. S. Roberts, P. F. Hollenberg, *J. Am. Chem. Soc.* **1995**, *117*, 12085–12091.
- [19] M. Newcomb, M.-H. Le Tadic, D. A. Putt, P. F. Hollenberg, *J. Am. Chem. Soc.* **1995**, *117*, 3312–3313.
- [20] M. Newcomb, R. Shen, Y. Lu, M. J. Coon, P. F. Hollenberg, D. A. Kopp, S. J. Lippard, *J. Am. Chem. Soc.* **2002**, *124*, 6879–6886.
- [21] K. Auclair, Z. Hu, D. M. Little, P. R. Ortiz de Montellano, J. T. Groves, *J. Am. Chem. Soc.* **2002**, *124*, 6020–6027.
- [22] N. Suzuki, T. Higuchi, T. Nagano, *J. Am. Chem. Soc.* **2002**, *124*, 9622–9628.
- [23] F. Ogliaro, N. Harris, S. Cohen, M. Filatov, S. P. de Visser, S. Shaik, *J. Am. Chem. Soc.* **2000**, *122*, 8977–8989.

- [24] N. Harris, S. Cohen, M. Filatov, F. Ogliaro, S. Shaik, *Angew. Chem. Int. Ed.* **2000**, *39*, 2003–2007.
- [25] S. P. de Visser, F. Ogliaro, N. Harris, S. Shaik, *J. Am. Chem. Soc.* **2001**, *123*, 3037–3047.
- [26] S. Shaik, S. P. de Visser, F. Ogliaro, H. Schwarz, D. Schröder, *Curr. Opin. Chem. Biol.* **2002**, *6*, 556–567.
- [27] S. P. de Visser, F. Ogliaro, P. K. Sharma, S. Shaik, *J. Am. Chem. Soc.* **2002**, *124*, 11809–11826.
- [28] P. K. Sharma, S. P. de Visser, F. Ogliaro, S. Shaik, *J. Am. Chem. Soc.* **2003**, *125*, 2291–2300.
- [29] K. Yoshizawa, Y. Kagawa, Y. Shiota, *J. Phys. Chem. B* **2000**, *104*, 12365–12370.
- [30] K. Yoshizawa, T. Kamachi, Y. Shiota, *J. Am. Chem. Soc.* **2001**, *123*, 9806–9816.
- [31] T. Kamachi, K. Yoshizawa, *J. Am. Chem. Soc.* **2003**, *125*, 4652–4661.
- [32] V. Guallar, B. F. Gherman, W. H. Miller, S. J. Lippard, R. A. Friesner, *J. Am. Chem. Soc.* **2002**, *124*, 3377–3384.
- [33] S. Shaik, M. Filatov, D. Schröder, H. Schwarz, *Chem. Eur. J.* **1998**, *4*, 193–199.
- [34] F. Ogliaro, S. Cohen, M. Filatov, N. Harris, S. Shaik, *Angew. Chem.* **2000**, *112*, 4009–4013; *Angew. Chem. Int. Ed.* **2000**, *39*, 3851–3855. Erratum: *Angew. Chem. Int. Ed.* **2001**, *40*, 647.
- [35] D. L. Harris, *Curr. Opin. Chem. Biol.* **2001**, *5*, 724–735.
- [36] M. T. Green, *J. Am. Chem. Soc.* **1999**, *121*, 7939–7940.
- [37] J. K. Atkinson, P. F. Hollenberg, K. U. Ingold, C. C. Johnson, M.-H. Le Tadic, M. Newcomb, D. A. Putt, *Biochemistry* **1994**, *33*, 10630–10637.
- [38] M. Newcomb, D. Aebischer, R. Shen, R. Esala, P. Chandrasena, P. F. Hollenberg, M. J. Coon, *J. Am. Chem. Soc.* **2003**, *125*, 6064–6065.
- [39] F. Ogliaro, S. P. de Visser, S. Cohen, P. K. Sharma, S. Shaik, *J. Am. Chem. Soc.* **2002**, *124*, 2806–2817.
- [40] P. K. Sharma, S. P. de Visser, S. Shaik, *J. Am. Chem. Soc.* **2003**, *125*, 8698–8699.
- [41] R. Davydov, T. M. Makris, V. Kofman, D. E. Werst, S. G. Sligar, B. M. Hoffman, *J. Am. Chem. Soc.* **2001**, *123*, 1403–1415.
- [42] S. Jin, T. M. Markis, T. A. Bryson, S. G. Sligar, J. H. Dawson, *J. Am. Chem. Soc.* **2003**, *125*, 3406–3407.
- [43] F. Hino, D. Dolphin, *Chem. Commun.* **1999**, 629–630.
- [44] T. G. Traylor, K. W. Hill, W.-P. Fann, S. Tsuchiya, B. E. Dunlap, *J. Am. Chem. Soc.* **1992**, *114*, 1308–1312.
- [45] F. Ogliaro, M. Filatov, S. Shaik, *Eur. J. Inorg. Chem.* **2000**, 2455–2458.
- [46] J. C. Schöneboom, H. Lin, N. Reuter, W. Thiel, S. Cohen, F. Ogliaro, S. Shaik, *J. Am. Chem. Soc.* **2002**, *124*, 8142–8151.
- [47] M. Filatov, N. Harris, S. Shaik, *Angew. Chem.* **1999**, *111*, 3730–3733; *Angew. Chem. Int. Ed.* **1999**, *38*, 3510–3512.
- [48] M. T. Green, EXAFS data presented at the *12th International Conference on Cytochrome P450*, La Grande Motte, France, September 11–15, **2001**.
- [49] S. P. de Visser, F. Ogliaro, P. K. Sharma, S. Shaik, *Angew. Chem. Int. Ed.* **2002**, *41*, 1947–1951.
- [50] J. T. Groves, Z. Gross, M. K. Stern, *Inorg. Chem.* **1994**, *33*, 5065–5072.
- [51] Z. Gross, S. Nimri, C. M. Barzilay, L. Simkhovich, *J. Biol. Inorg. Chem.* **1997**, *2*, 492–506.
- [52] J. C. Schöneboom, S. Cohen, H. Lin, S. Shaik, W. Thiel, manuscript in preparation.
- [53] F. Ogliaro, S. P. de Visser, S. Cohen, J. Kaneti, S. Shaik, *ChemBioChem* **2001**, *2*, 848–851.
- [54] P. E. M. Siegbahn, R. H. Crabtree, *J. Am. Chem. Soc.* **1997**, *119*, 3103–3113.
- [55] M. Torrent, D. G. Musaev, H. Basch, K. Morokuma, *J. Comp. Chem.* **2002**, *23*, 59–76.
- [56] E. J. Mueller, P. J. Loida, S. G. Sligar, in *Cytochrome P450: Structure, Mechanism and Biochemistry* (Ed.: P. R. Ortiz de Montellano) 2nd ed., Plenum Press, New York, **1995**, pp. 83–124.
- [57] K. E. Liu, C. C. Johnson, M. Newcomb, S. J. Lippard, *J. Am. Chem. Soc.* **1993**, *115*, 939–947.
- [58] S. P. de Visser, F. Ogliaro, S. Shaik, *Angew. Chem. Int. Ed.* **2001**, *40*, 2871–2874.
- [59] J. T. Groves, *J. Chem. Educ.* **1985**, *62*, 928–931.
- [60] A. H. C. Horn, T. Clark, *J. Am. Chem. Soc.* **2003**, *125*, 2809–2816.
- [61] D. Kumar, S. P. de Visser, S. Shaik, *J. Am. Chem. Soc.* **2003**, *125*, 13024–13025.
- [62] S. Shaik, A. Shurki, *Angew. Chem. Int. Ed.* **1999**, *38*, 586–625; *Angew. Chem.* **1999**, *11*, 616–657.
- [63] D. Kumar, S. P. de Visser, P. K. Sharma, S. Cohen, S. Shaik, *J. Am. Chem. Soc.*, in press.
- [64] F. Ogliaro, S. P. de Visser, S. Shaik, *J. Inorg. Biochem.* **2002**, *91*, 554–567.
- [65] F. Ogliaro, S. P. de Visser, J. T. Groves, S. Shaik, *Angew. Chem. Int. Ed.* **2001**, *40*, 2874–2878.
- [66] T. L. Poulos, *J. Biol. Inorg. Chem.* **1996**, *1*, 356–359.
- [67] F. Ogliaro, S. Cohen, S. P. de Visser, S. Shaik, *J. Am. Chem. Soc.* **2000**, *122*, 12892–12893.
- [68] P. H. Toy, M. Newcomb, M. J. Coon, A. D. N. Vaz, *J. Am. Chem. Soc.* **1998**, *120*, 9718–9719.
- [69] H. I. Liu, M. Sono, S. Kadkhodayan, L. P. Hager, B. Hedman, K. O. Hodgson, J. H. Dawson, *J. Biol. Chem.* **1995**, *270*, 10544–10550.
- [70] T. Kamachi, Y. Shiota, T. Ohta, K. Yoshizawa, *Bull. Chem. Soc. Jpn.* **2003**, *76*, 721–732.
- [71] S. P. de Visser, S. Shaik, *J. Am. Chem. Soc.* **2003**, *125*, 7413–7424.
- [72] Jaguar 4.1, Schrödinger, Inc., Portland, OR, **1991–2000**.
- [73] M. J. Frisch, G. W. Trucks, H. B. Schlegel, G. E. Scuseria, M. A. Robb, J. R. Cheeseman, V. G. Zakrzewski, J. A. Montgomery, Jr., R. E. Stratmann, J. C. Burant, S. Dapprich, J. M. Millam, A. D. Daniels, K. N. Kudin, M. C. Strain, O. Farkas, J. Tomasi, V. Barone, M. Cossi, R. Cammi, B. Mennucci, C. Pomelli, C. Adamo, S. Clifford, J. Ochterski, G. A. Petersson, P. Y. Ayala, Q. Cui, K. Morokuma, D. K. Malick, A. D. Rabuck, K. Raghavachari, J. B. Foresman, J. Cioslowski, J. V. Ortiz, A. G. Baboul, B. B. Stefanov, G. Liu, A. Liashenko, P. Piskorz, I. Komaromi, R. Gomperts, R. L. Martin, D. J. Fox, T. Keith, M. A. Al-Laham, C. Y. Peng, A. Nanayakkara, C. Gonzalez, M. Challacombe, P. M. W. Gill, B. Johnson, W. Chen, M. W. Wong, J. L. Andres, C. Gonzalez, M. Head-Gordon, E. S. Replogle, J. A. Pople, *Gaussian 98*, Gaussian, Inc., Pittsburgh PA, **1998**.
- [74] D. Danovich, “Green’s Function Method in Semiempirical Molecular Orbital Theory: Calculations of Ionization Potentials and Electron Affinities”, in *Encyclopedia of Computational Chemistry* (Eds.: P. v. R. Schleyer, N. L. Allinger, T. Clark, J. Gasteiger, P. A. Kollman, H. F. Schaefer III), John Wiley & Sons, **1998**, vol. 2, p. 1190–1202.
- [75] D. Danovich, Y. Apeloig, S. Shaik, *J. Chem. Soc., Perkin Trans. 2* **1993**, 321–329.

Received July 8, 2003